

Loss of Glyoxalase 1 Induces Compensatory Mechanism to Achieve Dicarbonyl Detoxification in
Mammalian Schwann Cells

Jakob Morgenstern¹, Thomas Fleming^{1,5}, Dagmar Schumacher², Volker Eckstein³, Marc Freichel²,
Stephan Herzig^{4,5}, Peter Nawroth^{1,4,5}

From the ¹Department of Internal Medicine I and Clinical Chemistry, University Hospital Heidelberg, Im Neuenheimer Feld 410, 69120 Heidelberg, ²Institute of Pharmacology, University of Heidelberg, Im Neuenheimer Feld 366, 69120 Heidelberg, ³Department of Medicine V, University Hospital Heidelberg, Im Neuenheimer Feld 410, 69120 Heidelberg, ⁴German Institute for Diabetes and Cancer (IDC), Helmholtz Center Munich, Ingolstädter Landstraße 1, 85764 Neuherberg, ⁵ German Center for Diabetes Research (DZD), Ingolstädter Landstraße 1, 85764 Neuherberg

Running title: Glyoxalase knock-out and compensatory mechanism

Keywords: Glyoxalase system, methylglyoxal, glycation, aldose reductase, diabetic neuropathy

ABSTRACT

The glyoxalase system is a highly specific enzyme system existing in all mammalian cells which is responsible for the detoxification of dicarbonyl species, primarily methylglyoxal (MG). It has been implicated to play an essential role in preventing the increased formation of advanced glycation endproducts under certain pathological conditions. We have established the first glyoxalase 1 knock-out model (GLO1^{-/-}) in mammalian Schwann cells using CRISPR/Cas9 technique to investigate compensatory mechanisms. Neither elevated concentrations of MG nor associated protein modifications were observed in GLO1^{-/-} cells. Alternative detoxification of MG in GLO1^{-/-} is achieved by increased catalytic efficiency of aldose reductase towards hemithioacetal (product of glutathione and MG), most likely caused by S-nitrosylation of aldose reductase. The hemithioacetal is mainly converted into lactaldehyde, which is paralleled by a loss of reduced glutathione. Inhibition of aldose reductase in GLO1^{-/-} cells is associated with an increased sensitivity against MG, elevated intracellular MG levels and associated modifications, as well as increased oxidative stress. Our data suggest that aldose reductase can compensate the loss of GLO1. This might be of clinical importance within the context of neuronal diseases caused by an impaired glyoxalase system and elevated levels of dicarbonyl species, such as MG.

Advanced glycation endproducts (AGEs) are formed by non-enzymatic glycation of proteins and lipids. AGEs are most likely a risk factor for the progression of late diabetic complications such as diabetic neuropathy (1, 2). Methylglyoxal (MG), a reactive dicarbonyl and major precursor for AGEs is derived from lipid peroxidation, threonine metabolism but mainly from glycolysis (3). Hyperglycemic episodes have been linked to increased formation of MG in animals and humans (4-6). MG and associated protein modifications induces cytotoxic effects through the initiation of cell growth arrest, apoptosis and production of reactive oxygen species (7).

One way to detoxify this reactive metabolite is via the highly specific glyoxalase system, conserved from crude prokaryotics to complex mammalian organisms. The major substrate for the first enzyme in the system, glyoxalase 1 (GLO1), is the non-enzymatically formed product of MG and reduced glutathione (GSH). This spontaneously produced hemithioacetal (HTA) is converted to S-D-lactoylglutathione, which is then hydrolyzed to D-lactate and GSH through the catalytic activity of glyoxalase 2 (8). In comparison to other enzymatic systems involved in the detoxification of endogenous toxins, the glyoxalase system has a limited substrate specificity and is not depleting its cofactor, GSH. As the intermediate S-D-lactoylglutathione is a non-toxic metabolite, GLO1 represents the rate limiting step for the

detoxification of MG and thereby also for its toxic capacity (9). It highlights the importance of the glyoxalase system and the common opinion, that GLO1 is indispensable to maintain cellular viability (9, 17, 46). It has been shown that GLO1 has a reduced capacity in diabetic mice models and patients, which was paralleled by an accumulation of MG and MG specific AGEs, particularly in neuronal tissue (4, 10, 11, 56). MG-modified proteins in peripheral neurons, like voltage-gated sodium channels, can change the firing patterns of action potentials and consequently the mediation of mechanicals triggers like pain in patients suffering from diabetic neuropathy (18). It has been shown previously that sciatic nerves are highly susceptible to the accumulation of MG associated modifications in diabetes (51). Recently the critical role of Schwann cell metabolism has been described extensively and that its disruption can cause axonal degeneration. Furthermore the same study postulated that metabolic dysfunction in the Schwann cell-rich sciatic nerves is associated with the development of neuropathic symptoms in an experimental model of diabetes (49). Schwann cells are critical for the support, development and regeneration of peripheral neurons. However, there are very few studies which have investigated MG metabolism in these cell types.

Within the context of an alternative detoxification of MG only some studies have focused on enzymes of the aldehyde dehydrogenase family (ALDH) and aldo-keto reductase family (AKR). Both families have been claimed to convert MG into non-toxic compounds (12). The NADPH-dependent enzymes, such as aldehyde reductase (AKR1a1) and aldose reductase (AKR1b1 / AKR1b3), isolated from human placenta and skeletal muscle, are able to convert MG into hydroxyacetone and lactaldehyde (12, 13). *In vivo* data has confirmed the essential role of AKRs under diabetic conditions in cardiovascular tissue, wherein AKR1b3 null mice had increased AGEs in the heart and showed more atherosclerotic lesion formation (14). ALDHs on the other hand are NADH-dependent enzymes and several subtypes (ALDH1, 2, 3 and 9) should be able to convert MG into pyruvate (12, 15). However, the relative contribution to ALDHs to the detoxification of MG *in vivo* remains unknown. Deglycase DJ-1, also known as Parkinson disease protein 7 can convert MG without GSH directly

into lactate in mammalian cells (16). Due to a very low catalytic efficiency as compared to GLO1 (~1000 fold) the contribution of this enzyme in the context of MG detoxification is uncertain (9, 16). One of the major limitations of these studies is that the efficiency to detoxify MG has been investigated using either purified or recombinant proteins. However, the different expression levels of ALDHs and AKRs in various tissues indicate the difficulty in defining their relative contribution in detoxifying MG *in vivo*. It is notable that several inhibitors of aldose reductase (AKR1b3) have been used in clinical trials to treat patients suffering from neuropathic symptoms (42, 43). The inhibition of this enzyme to prevent the harmful accumulation of sorbitol in neuronal cells can theoretically have an adverse side effect, given the background of an potentially AKR1b3 driven detoxification of dicarbonyls.

The aim of this study therefore was to look at compensatory mechanisms in a neuronal research model system with a GLO1 deficiency. Within this context we expected to show that an alternative enzyme can process dicarbonyl species and those findings could contribute to improve the molecular understanding of specific neuropathy disorders.

RESULTS

Loss of GLO1 is not associated with increased levels of methylglyoxal or modified proteins—Effective detoxification of MG is mainly accomplished by the glyoxalase system. We established a permanent loss of GLO1 protein and GLO1 activity in murine Schwann cells (Table 1 and Fig. 1A). To investigate the consequences of a GLO1 knock-out under baseline conditions, we determined the levels of MG and MG specific protein modifications. We detected neither an increase in intracellular MG-levels nor MG associated protein modifications (Fig.1, B, C and D). To establish the enzymes potentially involved in the alternative detoxification we analyzed the mRNA content of 10 AKR and 9 ALDH subtypes in wild-type & GLO1^{-/-} Schwann cells with and without exposure to MG. The results revealed a baseline upregulation of 2 subtypes of AKRs (1a1, 1b3) and 2 ALDHs (1a2, 1a3) (Fig. 2A). After the exposure to MG the mRNA content of AKR1b3 and AKR1b8 were further increased in GLO1^{-/-} Schwann cells (Fig. 2B). In wild-type Schwann

cells the exposure to MG increased the expression of 3 ALDH subtypes (1a2, 1a3, 3a2) significantly.

S-Nitrosylation of AKR1b3 is beneficial for the efficient detoxification of dicarbonyl species in GLO1^{-/-} Schwann cells—To assess the contribution of the upregulated enzymes we determined kinetic profiles for the ALDHs and AKRs present in the cytosolic fractions of GLO1^{-/-} Schwann cells. When MG and the appropriate co-factor (NADPH or NADH) were added as substrate, V_{\max} for AKR was 0.654 $\mu\text{mol NADPH/s/mg Protein}$, while the V_{\max} for ALDH was only 0.088 NADP/s/mg Protein (Fig. 3A), suggesting that only enzymes of the AKR family are able to detoxify MG efficiently in GLO1^{-/-} Schwann cells. Comparison of AKR kinetics with wild-type Schwann cells revealed the same efficiency in catalyzing the conversion of MG (Fig. 3B). When HTA (non-enzymatic product of MG and GSH) was used in the same enzymatic assay as a substrate, capacity and affinity were increased in GLO1^{-/-} Schwann cells as compared to wild-type Schwann cells (Fig. 3C). This observation was not caused by an increased amount of the most abundant AKR subtype AKR1b3 in GLO1^{-/-} Schwann cells (Fig. 3D).

To investigate the reason for the increased catalytic activity in GLO1^{-/-} Schwann cells towards the substrate HTA we detected higher intracellular levels of nitric oxide (NO) and higher amounts of nitrosylated cystein residues in GLO1^{-/-} Schwann cells (Fig. 4, A and C). Analysis of the mRNA expression of all NOS subtypes revealed that NOS2 or iNOS as the driving force for increased nitric oxide species in GLO1^{-/-} Schwann cells (Fig. 4D). The specific inhibition of this isoform was associated with increased MG-levels and MG modified proteins in 2 of the GLO1^{-/-} Schwann cell clones (Fig. 4, E and G) and also with a decreased tolerance against exogenously added MG in a toxicity assay (Fig. 4F). Additionally we found that the exposure to relative low MG concentrations (50 μM) was accompanied by increased levels of NO, NOS activity and S-Nitrosylation in GLO1^{-/-} Schwann cells (Fig. 4, A, B and C)

The incubation of recombinant AKR1b3 with an NO-donor (Streptozotocin) revealed a ~2-fold increased activity towards HTA as a substrate as compared to the unmodified recombinant AKR1b3 (Fig. 4, H and I).

AKR1b3 has an essential role in maintaining cellular viability and preventing accumulation/formation of MG & MG modified proteins and oxygen species—To investigate the contribution of AKR1b3, we determined the median lethal dose (LD₅₀) for MG under different conditions. Wild-type Schwann cells had a baseline LD₅₀ of $220 \pm 19 \mu\text{M MG}$ regardless if they have been treated with an AKR1b3 inhibitor (Epalrestat) (Fig. 5B). In 3 individual GLO1^{-/-} Schwann cell clones the baseline tolerance against MG was decreased to an LD₅₀ of $69 \pm 3.7 \mu\text{M MG}$ (Fig. 5B). The treatment with an AKR1b3 inhibitor (Epalrestat) or the usage of siRNA against AKR1b3 was accompanied by almost a total loss of MG tolerance (AKR1b3 siRNA: LD₅₀ = 31.6 ± 9.2 ; Epalrestat: LD₅₀ = 14.2 ± 8.6) (Fig. 5B). The overexpression of AKR1b3 in 3 individual GLO1^{-/-} Schwann cell clones could prevent the decreased tolerance towards MG (AKR1b3 OE: LD₅₀ = $118.1 \pm 29.8 \mu\text{M}$), whereby the treatment of Epalrestat parallely diminished this rescue effect (Fig. 5B). The inhibition of AKR1b3 with Epalrestat was associated with significantly increased levels of MG and MG modified arginine residues in all 3 GLO1^{-/-} Schwann cell clones (Fig. 5, A and C). Additionally we found elevated levels of hydrogen peroxide (2-fold) and superoxide species (3-fold) following AKR1b3 inhibition with Epalrestat in GLO1^{-/-} Schwann cells (Fig. 5D).

GSH reductase is required to preserve cellular GSH concentration in GLO1^{-/-} Schwann cells and to assist in the detoxification of dicarbonyl species—As GSH is a fundamental cofactor in the context of MG detoxification, its fate after the conversion of HTA in wild-type and GLO1^{-/-} Schwann cells was investigated. Both cell lines were exposed to HTA and the GSH/GSSG content was determined at different time points. In the wild-type Schwann cells a slight increase of GSH after 20 minutes was detectable, whereas the GSSG content showed no change over the whole time period (Fig. 6, A and B). In 3 individual GLO1^{-/-} Schwann cell clones, GSH was rapidly diminished after the exposure to HTA. This was paralleled by an increase in GSSG, which was equalized 60 minutes after the exposure with HTA (Fig. 6, A and B).

Analysis of the activity and the protein content of GSH reductase revealed a ~2-fold increase of both in GLO1^{-/-} Schwann cells (Fig. 6, C and D). In wild-type and GLO1^{-/-} Schwann cells the inhibition

of GSH reductase was paralleled with a decrease in GSH (Fig. 6E). Only in GLO1^{-/-} Schwann cells was this inhibition associated with enhanced GSSG levels (Fig. 6F).

However, the inhibition GSH reductase was not associated with a decreased tolerance towards MG in GLO1^{-/-} Schwann cells (Fig. 6H). Within the context of MG metabolism this inhibition of GSH reductase led only to a minor and none significant increase in MG, but to an significant increase in MG modified proteins in 3 individual GLO1^{-/-} Schwann cells (Fig. 6, G and I). Additionally the inhibition of GSH reductase was accompanied with a increase of both oxygen species in wild-type and GLO1^{-/-} Schwann cells (Fig. 6J).

Products of alternative detoxification are hydroxyacetone and lactaldehyde—To determine the products of this alternative detoxification pathway, labeled d4-MG was used. In wild-type Schwann cells the most abundant peak was d4-D-lactate paralleled by a slight increase in d4-hydroxyacetone (Fig. 7, A and C). Incubation of cytosolic fractions from GLO1^{-/-} Schwann cells with d4-MG revealed no abundance of d4-D-lactate, but an increase in d4-hydroxyacetone and d4-lactaldehyde (Fig. 7B). The distribution for those products was in favor of lactaldehyde (90 %) (Fig. 7C).

DISCUSSION

Schwann cells are responsible for many aspects of peripheral nerve biology, such as maintenance of axonal integrity, insulation of axons, localization of sodium channels and nerve regeneration. In diabetic neuropathy most of those aspects are malfunctioning (39, 50). Increased oxidative stress caused by reactive compounds, deriving from a disturbed energy metabolism, contributes to the dysfunction of Schwann cells. The inefficient detoxification of those reactive compounds, such as MG, may indirectly be linked to the progression of diabetic neuropathy (52).

The glyoxalase system has been shown to have a key role in preventing the harmful events of glycated proteins and lipids via the removal of dicarbonyl species (7, 9, 35). The knock-down of GLO1 was associated with diabetic nephropathy in healthy wild-type mice and a decreased capacity of GLO1 resulted in dramatic accumulation of MG in diabetic patients (21, 6). The overexpression of GLO1, on the other hand, could prevent the accumulation of MG and AGEs and has shown

cyto-protective effects *in vitro* and *in vivo* (17, 19). Recent research has focused on the development of inducers for GLO1 activity and first clinical trials have taken place for the establishment of a GLO1 enhancer in diabetic patients (22, 48). The attention paid to this topic therefore highlights the importance of GLO1 in preventing the progression of diabetic complications.

Surprisingly in our GLO1^{-/-} model system we detected neither elevated MG nor MG specific protein modifications. This can be explained by a highly efficient AKR1b3 which tries to imitate GLO1 in catalyzing excessive amounts of HTA, the spontaneous product of MG and GSH. The higher catalytic efficiency of GLO1^{-/-} Schwann cells in converting HTA is likely due to a post-translational modification of AKR1b3. The upregulation of iNOS and increased NO-levels are paralleled by elevated amounts of nitrosylated cysteine residues. Interestingly it has been shown frequently that MG can impair NO homeostasis and this has been related to endothelial dysfunction via a modulation of eNOS (60, 61). The increased generation of NO in endothelial cells was also related to the production of peroxynitrite and therefore to the harmful effect of NO concluded the authors (62). In our study recombinant AKR1b3 which has been nitrosylated *ex vivo* showed the same increased kinetic efficiency towards HTA similar to the GLO1^{-/-} Schwann cells. It was also shown that exogenous MG increased the intracellular levels of NO even further and in turn the inhibition of iNOS was associated with an impaired MG metabolism. Given this background we have strong indications for a NOS driven post-translational modification of AKR1b3, which leads to a more efficient catalysis of GSH bound MG (HTA). Indeed the S-nitrosylation of AKR1b3 at Cys298 and Cys303 has been described elsewhere and is associated with an increased activity of the enzyme which can be reversed by glutathiolation (36, 37). Within this context, it is interesting to note that the conversion of HTA by AKR1b3 in GLO1^{-/-} Schwann cells was paralleled by an intracellular change in the ratio of oxidized/reduced GSH, potentially caused by the necessity for a glutathiolation of nitrosylated AKR1b3 to reverse it into a reduced form. The inhibition of GSH reductase showed that GSSG levels are rising rapidly in GLO1^{-/-} Schwann cells. It seems to play a crucial role in those cells to

maintain the intracellular GSH pool in a range to prevent cell death.

However, GLO1^{-/-} Schwann cells would have an increased demand for reducing agents like NADPH. This is on the one side a result of the alternative detoxification through AKR1b3, and on the other due to the reduction of oxidized GSH. Generation of reducing agents is only achievable with an increased glycolysis, particularly with the pentose phosphate way. Consequently this would lead to increased reactive oxygen species and MG production which causes the necessity for even more reducing agents like NADPH, leading to a vicious circle.

Vander-Jagt *et al.* had previously shown that AKR1b3 can act as an aldehyde-reducing enzyme or a ketone-reducing enzyme, resulting in the production of hydroxyacetone and lactaldehyde, respectively. (12, 23). In our study we confirmed this data *in vivo* using isotopically labeled d4-MG. The existence of ~2% d4-hydroxyacetone in wild-type Schwann cells after the conversion of d4-MG indicates that the contribution of alternative detoxification through AKR1b3 is minimal in healthy wild-type Schwann cells. In GLO1^{-/-} Schwann cells the main product is lactaldehyde due to a change in substrate specificity of AKR1b3. Previous studies which have focused on alternative enzymes for the detoxification of MG were based upon the idea that free unhydrated MG will be detoxified directly through alternative enzymes into hydroxyacetone or pyruvate, depending on the tissue distribution of AKRs and ALDHs (12, 15). However, the intracellular GSH concentrations are kept in a range which is 100-fold higher than cytosolic MG concentrations (23). This guarantees an immediate binding of MG to GSH to form the substrate of GLO1. As GSH is present in excessive amounts in the cytosol and HTA has a dissociation constant of ~3mM, free MG can only exist in low nanomolar traces in the cytosol, suggesting its concentration is below the lowest affinity of AKRs and ALDHs (24, 25, 47).

AKR1b3 or commonly known as aldose reductase is a ubiquitously expressed enzyme, especially in cells of the kidney and the peripheral nervous system. It is a catalyst with a broad range of substrates with physiological significance, such as 4-hydroxynonenal, isocorticosteroids, glutathione conjugates or pollutants like acrolein (20). Much attention has been paid to this protein

for its crucial role as the initial enzyme of the polyol pathway, where it produces sorbitol during hyperglycemic episodes in various tissues (38, 39). Glucose is preferentially taken up into Schwann cells in peripheral neurons, which have naturally high expression levels of AKR1b3 compared to cells of other tissues (40, 41). This is the reason why a lot of efforts have been made in the last two decades to develop AKR1b3 inhibitors in order to prevent diabetic complications caused by high sorbitol levels (42). However, the results of a large number of new therapies tested in clinical trials and animal experiments are contradictory. From nine AKR1b3 inhibitors only epalrestat showed slightly beneficial and non-adversarial health effects, and is only marketed for usage in Japan and India and not in the US or European Union (43, 44). In this study we have demonstrated that the inhibition of AKR1b3 by epalrestat, when GLO1 is lost, is associated with increased MG concentration and elevated AGE levels. It is therefore conceivable that in diabetes, the loss of GLO1 activity leads to the detoxification of MG by AKR1b3. Within this context, the inhibition of AKR1b3, far from preventing the accumulation of sorbitol, blocks the remaining pathway by which other reactive metabolites can be detoxified, leading to their accumulation and increased post-translational modifications. The double-edged role of AKR1b3, in activating the polyol pathway on the one side, and detoxifying reactive metabolites on the other is paradoxical and has to be investigated in further studies. However, our study provides a mechanism to explain why several AKR1b3 inhibitors have failed in clinical trials for the treatment of diabetic complications. It shows for the first time a way to survive dicarbonyl mediated stress without the glyoxalase system in mammalian cells. Although the cells are highly susceptible to exogenously added MG, the intracellular MG concentrations of GLO1^{-/-} Schwann cells are held in a range similar to wild-type cells. Undoubtedly, AKR1b3 contributes to the detoxification of AGE precursors in cells of the peripheral nervous system while GLO1 is not as efficient as it should be. Within a clinical context where GLO1 activity is reduced such as in diabetic and elderly patients there is no clear cut relationship between patient outcome and GLO1 activity. This fact potentially indicates the existence of an alternative pathway for MG

detoxification or the possibility that a low expression of GLO1 is sufficient.

EXPERIMENTAL PROCEDURES

Cell culture—Primary murine Schwann cells immortalized with SV40 large T antigen were obtained from ATCC® (Mannassas, Virginia). Cells were grown in DMEM (gibco) with 1 g/mL glucose containing 10% FCS (Sigma), 1% penicillin (10000 Units/ml) (gibco), 1% streptomycin (10 mg/ml) (gibco) and 1% amphotericin B (250 µg/ml) (gibco) at 33°C in a saturated humidity atmosphere containing 95% air and 5% CO₂. Cells were grown to 70% confluence for in vivo experiments and passaged at 90% confluence using 0.05% Trypsin-EDTA (gibco).

Synthesized chemicals—MG solution (40% w/v) was purchased from Sigma. d4-MG was synthesized, as previously described (53), using d6-Acetone. The concentration of MG was determined by LC-MS/MS, as described. The concentration and purity of the stock solutions were determined by ¹³C- and ¹H-NMR using a Bruker Avance II NMR spectrometer. The total purity of the unlabelled and labelled MG solutions was 60-65% with the major contaminants being methanol, acetate and acetone.

Antibody against MG-H1—A rat monoclonal antibody against MG-H1 was developed in collaboration with the monoclonal antibody core facility at Helmholtz Centre in Munich. Briefly, a peptide-based antigen was synthesized which contained a single, chemical defined MG-H1 residue (54). Following immunization of LouC rats with ovalbumin-coupled MG-H1-modified peptide, hybridomas were generated according to the standard procedures. Hybridomas were screened for reactivity towards the MG-H1-peptide antigen, and human serum albumin modified minimally with MG by ELISA and western blotting (55). Positive wells were established and cloned twice by limiting dilution. One anti-MG-H1 monoclonal antibody recognizing MG-H1 was designated 6D7 (IgG2c) was used in the present study as culture supernatant. A more detailed characterization of the anti-MG-H1 antibody will be published elsewhere.

Generation of CRISPR/Cas9-induced Glo1 knockout cells—Four sgRNAs (76; 171; 183; 187) targeting exon1 and 2 of the Glo1 locus were designed and cloned into an U6-promoter driven

expression vector (pU6-gRNA) by Sigma. All sgRNAs were tested for efficiency by transfecting together with the Cas9-expressing plasmid pX330-U6-Chimeric_BB-CBh-hSpCas9 (Addgene plasmid ID: 42230) into C3H/10T1/2 mouse embryonic cells. After 72h, DNA was extracted using a QIAGEN QIAamp® DNA Mini Kit. T7 endonuclease assay using T7 Endonuclease I (New England Biolabs) was performed with primers flanking the modified site. sgRNA171 revealed the most efficient performance with a gene editing efficiency of 37% (specific recognition site: 5'-AGCACCAAGGTGGGTGAC3'). GLO1 deficient Schwann cells were established by transfecting with sgRNA171, plasmid pX330 and mTurquoise-expressing plasmid (kind gift from Dr. Joachim Goedhart (34)) using a NEON® electroporation transfection system (Thermo) with the following conditions; pulse voltage: 1,300 mV, pulse width: 20 ms, pulse number: 2. Schwann cells were either transfected with an empty plasmid containing only an mTurquoise vector (wild-type) or with the plasmid containing mTurquoise, sgRNA_171 and pX330 (GLO1^{-/-}). Transfected cells were then sorted as single cells by FACSariaII (BD Bioscience). Positive transfected cells were detected by ultraviolet laser (Excitation: 355 nm; Filter: 379/28 nm) and were then cultured as sorted single cells and grown to 80% confluence before subculturing. In total 19 clones based on a single cell seeding strategy were cultured and analyzed for GLO1 activity and protein expression. Based upon the sequencing analysis, clone #1, #3 and #4 were chosen for experiments, which were then renamed to #1, #2 and #3 in the results section for a better understanding. The methods and the sequencing results for those 3 individual clones are summarized in a supplemental file.

Overexpression/Silencing of AKR1b3 in GLO1^{-/-} Schwann cells—Host *E.coli* strain DH10B including a mammalian expression vector (pCMV-SPORT6) for AKR1b3 (GE Healthcare; Clone ID: 3582788; Insert Sequence: BC004725) was plated out on LB-plates including 100 µg/ml ampicillin and incubated overnight at 37°C. Three individual clones were picked and amplified in LB broth including antibiotics for 12 h at 37°C and isolated using GenElute™ HP Plasmid MaxiPrep Kit (Sigma). Integrity of purified expression constructs was validated by gel electrophoresis and the concentration was determined by absorbance measurement. 1x10⁶ GLO1^{-/-} Schwann cells were

transfected with 20 µg of AKR1b3-vector using a NEON® electroporation transfection system (Thermo) with the conditions described above. Specific AKR1b3 downregulation / silencing was achieved using siGENOME AKR1b3 siRNA (GE Healthcare; RNA Accessions: NM_009658.3; Protein Accessions:NP_033788.3). Control groups (MOCK siRNA) were transfected with siGENOME Non-Targeting siRNA Pool (GE Healthcare; target firefly luciferase mRNA U47296). 1x10⁶ GLO1^{-/-} Schwann cells were transfected with 500 pmol of siRNA using a NEON® electroporation transfection system (Thermo) with the conditions described above. For both transfection approaches cells were allowed to acclimatize for 6h and then used for further experiments. Efficiency was assessed by Western blot 24h after treatment.

Quantitative PCR—Extraction of RNA was achieved using a peqGOLD MicroSpin Total RNA Kit (Peqlab), which was then converted into cDNA with a High-Capacity cDNA Reverse Transcription Kit (Thermo). qPCR was performed using DyNamo ColorFlash SYBR Green qPCR Master Mix (Thermo) and a LightCycler® 480 Instrument II (Roche). Signals of amplified products were verified using melting curve analysis and mRNA levels were normalized to Beta-Actin. Relative expression levels were calculated using the $\Delta\Delta C_t$ method described elsewhere (59). Primer sequences used for analyzing mRNA content were: AKR1a1 (PrimerBank ID: 10946870a1), forward `5-AGCCTGGTCAGGTGAAAGC-3` and reverse `5-GGCCTCCCAATCTCAGTT-3`; AKR1b3 (PrimerBank ID: 31981909a1), forward `5-AGGCCGTGAAAGTTGCTATTG-3` and reverse `5-ATGCTCTTGTATGGAACGTG-3`; AKR1b8 (PrimerBank ID: 6679791a1), forward `5-GACCAAGGCAGAATCCTCACC-3` and reverse `5-AGATGCCCTTCGAGTGACAGT-3`; AKR1c1 (PrimerBank ID: 13386240a1), forward `5-TTGGAACAATCCCTGAGAAAGC-3` and reverse `5-TGGCTAACCTGAATCCTTACA-3`; AKR7a5 (PrimerBank ID: 27659728a1), forward `5-CGGCCAGTCCGAGAACATC-3` and reverse `5-TTCAGTGACTTCCCTTCCCAG-3`; ALDH1a2 (PrimerBank ID: 6677665a1), forward `5-CAGAGAGTGGGAGAGTGTTC-3` and reverse `5-CACACAGAACCAAGAGAGAAGG-3`; ALDH1a3 (PrimerBank ID: 31542123a1), forward `5-GGGTCACACTGGAGCTAGGA-3`

and reverse `5-CTGGCCTCTTCTTGGCGAA-3`; ALDH3a2 (PrimerBank ID: 6680678a1), forward `5-TCTCTGCCCTTTGGAGGTGT-3` and reverse `5-AGCTGATCCTTGACAATCACAG-3`; NOS1 (PrimerBank ID: 6724321a1), forward `5-CTGGTAAGGAACGGGTCAG-3` and reverse `5-CCGATCATTGACGGCGAGAAT-3`; NOS2 (PrimerBank ID: 6754872a1), forward `5-GTTCTCAGCCCAACAATAACAAGA-3` and reverse `5-GTGGACGGGTCGATGTCAC-3`; NOS3 (PrimerBank ID: 31982150a1), forward `5-GGCTGGGTTTAGGGCTGTG-3` and reverse `5-CTGAGGGTGCGTAGGTGATG-3`.

Preparation of total/cytosolic protein extracts—For cytosolic extracts 500 µl cold lysis-buffer (10 mM HEPES, 1.5 mM MgCl₂, 10 mM KCl, 0.5 mM DTT, 0.05% NP40 supplemented with a premade protease inhibitor cocktail (Sigma) including AEBSF, Aprotinin, Bestatin, E-64, Leupeptin, Pepstatin A) was added to 3x10⁶ cells. Samples were then homogenized by passing the lysate 20 times through a 20G needle. After centrifugation (8000 rpm, 10 min, 4°C) the supernatant was used for protein determination and further analysis. For total extracts 500 µl of cold Radioimmunoprecipitation buffer (RIPA; 50 mM Tris-HCl; pH 7.5, 150 mM NaCl, 1% NP40, 0.5% sodium deoxycholate, 0.1% SDS, 0.5 mM DTT, 1000 units benzonase and supplemented with a premade protease inhibitor cocktail (see above) was added to 3x10⁶ cells. Samples were vortexed and sonicated for 30 seconds (50% power, 3 cycles) with an ultrasonic homogenizer HD2070 (Bandelin). After 30 min of incubation samples were centrifuged (14000 rpm, 10 min, 4°C) and supernatant was used for protein determination and further analysis. All protein concentrations were determined using the Bradford technique and BSA as calibration standard as described previously (31).

Western blotting—20 µg protein was incubated in 2x Laemmli buffer (Sigma) at 95°C for 10 min and separated by a Mini-PROTEAN® TGX (Bio-Rad) precasted gel (4-20% acrylamide). Proteins were then transferred to a nitrocellulose membrane and blocked with 2% dry milk (in PBS) or in the case of protein modifications with a Pierce® protein-free blocking buffer (Thermo) at room temperature for 1 h. Membranes were then incubated overnight at 4°C with antibodies against GLO1 (1:1000 dilution; ab81461; rat; Abcam), GSH

reductase (1:1000 dilution; ab16801; rabbit; Abcam), aldo-keto reductase 1b1 (1:1000 dilution; ab175394; rabbit; Abcam) Beta-actin (1:2500 dilution; 4967S; rabbit; Cell Signaling Technology) in 2% dry milk containing PBS and 0.05% Tween20 (PBS-T). After 3 washing steps (5 min each) with PBS-T membranes were incubated with horseradish-linked goat anti-rat (1:2000 dilution; 7077S; Cell Signaling Technology) or goat anti-rabbit (1:2000 dilution; 7077S; Cell Signaling Technology) antibody for 1h at room temperature. Proteins were visualized on X-Ray films using ECL detection reagents (GE healthcare) with varying exposure time (0.1 – 2 min). Protein expression was determined using a densitometry analysing software QuantityOne (BioRad) and normalized to β -Actin expression.

Methylglyoxal toxicity assays—Viability assays were performed with 3-(4,5-dimethylthiazol-2-yl)-2,5-diphenyltetrazolium (MTT-method) as previously described with some minor changes (28). Cells were seeded into 96-well plates and grown to 80% confluency under basal growth conditions. Cells were then customized to DMEM medium with only 0.1% FCS for 24h and afterwards exposed to increasing concentrations of MG (10 - 500 μ M) for 48h. For viability determination 50 μ l of MTT solution (2 mg/ml in PBS) was added to the medium and cells were incubated at 33° for 2h. Reduced MTT was then solubilized in 200 μ l DMSO and absorbance was measured at 590 nm (reference at 690 nm) using a FLUOstar OMEGA multiplate reader (BMG Labtech). Viability was calculated as a percentage of controls (untreated cells). Data were fitted by nonlinear regression using the Graphpad PRISM 6 software (GraphPad Software Inc.) and values of LD₅₀ determined.

Determination of intracellular GSH and GSSG—Cells were exposed to 0.2 mM HTA for 10, 20, 30, 60, 90, 120 min. HTA was prepared according the K_d equations calculated before (47). Quantitative analysis of glutathione and glutathione disulfide were performed using an enzymatic recycling method as described previously (30).

Detection of S-nitrosylation and production of S-nitrosylated AKR1b3—S-nitrosylation was detected by iodoTMT switch technique, a modification of the biotin switch technique described elsewhere (45) using a

Pierce™ S-nitrosylation western blot kit (Thermo), according to the manufacturer's instructions. For the nitrosylation of recombinant AKR1b3, streptozotocin was used as an NO-donor (57). To 1 μ g of recombinant protein in sodium phosphate buffer (0.1 M; pH 7.2) 0.1 mmol streptozotocin was added and incubated for 30 min at room temperature and daylight. S-nitrosylated recombinant protein was washed and purified using a spin filter column with 3 kDa cut-off (Millipore). Nitrosylation of recombinant AKR1b3 was confirmed by western blot.

Enzymatic activity assays—Activity of GLO1 was determined spectrophotometrically as described previously (31). Briefly, the method monitors the initial rate of change in absorbance at 235 nm caused by the formation of S-D-lactoylglutathione through catalysis of GLO1. The assay mixture contained 2 mM MG and 2 mM GSH in sodium phosphate buffer (50 mM, pH 6.6, 37°C) and was incubated for 15 min to guarantee the complete formation of HTA. After the addition of the cytosolic protein fraction (1 μ g/ μ l) the change in absorbance was monitored for 15 min. The activity of GLO1 described in units (U), where 1 U is the amount of GLO1 which catalyzes the formation of 1 μ mol of S-D-lactoylglutathione per minute.

The kinetic activity assay for AKR in cytosolic fractions was performed as described previously with minor changes (33). Briefly, activity was determined in 0.1 M sodium phosphate buffer (pH 7.2) containing MG or HTA (0.1 – 2 mM) and 0.1 mM NADPH at 25°C. The reaction was monitored by following the loss of NADPH at 340 nm. ALDH activity was assayed at 25°C in 75 mM Tris-HCl (pH 9.5) containing 10 mM DL-2-amino-1propanol, 0.5 mM NADP and 0.1 - 2 mM MG by measuring the rate of NADP formation at 340 nm (12). Activity for GSH reductase was determined as described previously (58). For all kinetic analysis data were fitted by nonlinear regression using the Graphpad PRISM 6 software (GraphPad Software Inc.) and K_m and V_{max} were calculated. Activity for nitric oxide synthase (NOS) was determined using a commercially available kit (biovision). In this assay NO generated by NOS reacts with a fluorescent probe to generate a signal at Ex/Em = 360/450 nm, which is proportional to NOS activity.

Conversion of labeled d4-MG by wild-type and GLO1^{-/-} Schwann cells—Product analysis was achieved by exposing wild-type and GLO1^{-/-} Schwann cells with 150 μ M d4-MG (in DMEM medium with 0.1% FCS). Cells were then treated with 1 ml ice-cold PBS and harvested using a cell scraper (gibco). After the addition of 100 μ l of trichloroacetic acid (20% w/v in 0.9% NaCl) lysates were vortexed and sonicated for 30 seconds (50% power, 3 cycles). After a short spin down (14000 rpm, 5 min, 4°C) supernatant was stored at -20°C or used directly for further LC-MS/MS analysis.

Determination of metabolites via LC-MS/MS—hydroxyacetone, lactaldehyde and lactate were determined using O-(2,3,4,5,6-pentafluorophenyl) methyl hydroxylamine (PFBHA) as a derivatizing agent as described previously, with some changes (26). Supernatants (900 μ l) from the previous method description were used for derivatizing procedure (addition of 50 μ l of PFBHA (5 mM) for 2h at room temperature). After derivatizing procedure 10 μ l of sulfuric acid was added to bind excessive PFBHA. Mixture was then mixed with 600 μ l n-hexane which was isolated and evaporated using a vacuum concentrator (Savant SpeedVac™ SC100) at room temperature. Derivatized compounds were resolved in 100 μ l of a H₂O:Acetonitrile mixture (50:50) and used for LC-MS/MS analysis.

An Aquity UPLC class 1 liquid chromatography system (waters®) was used and analytes were separated by reverse-phase LC on a waters® Aquity BEH C18 column (1,7 μ M, 2,1 x 50 mm) at a flow rate of 0,3 ml/min and a column temperature of 40°C. Gradient elution was performed using solvent A (99.9% water + 0.01% formic acid) and B (99.9% acetonitrile + 0.01% formic acid). Gradient elution was performed with a total run time of 1h to guarantee a separation of components with the same mass. The gradient started with 90% A and was increased to 90% B over 50 min, and then held at 90% B for 5 min. The detection was carried out on a XEVO TQ-S tandem quadrupole mass spectrometer (waters®) using positive electrospray ionization mode. Analyte detection was performed using multiple reaction monitoring (MRM). Source parameters were set as follows: capillary voltage – 3.8 kV; desolvation temperature – 300°C; desolvation gas flow – 850 L/h; source temperature – 150°C; cone gas flow 250 L/h; collision gas flow – 0.15 mL/min; nebuliser gas flow – 5 bar. Identification

was based upon retention times, two MRM transitions for each compound (qualifier and quantifier) and the final comparison of values from spiked standards. MRM transitions used and retention times were: hydroxyacetone (m/z 270.1>252.1 & m/z 270.1>181.1), (retention time: 23.88 min); d4-hydroxyacetone (m/z 274.1>256.1 & m/z 274.1>181.1), (retention time: 23.86 min); D/L-lactate (m/z 284.2>266.1 & m/z 284.2>181.1), (retention time: 18.42 min); d4-D/L-lactate (m/z 288.2>270.1 & m/z 288.2>181.1), (retention time: 18.43 min); lactaldehyde (m/z 270.1>252.1 & m/z 270.1>181.1), (retention time: 25.19 min); d4-lactaldehyde (m/z 274.1>256.1 & m/z 274.1>181.1), (retention time: 25.17 min). Identification of products after the conversion of d4-MG was based on the comparison of retention times and the expected mass transitions of non-deuterated spiked calibrators. Acquisition and quantification was completed with MassLynx 4.1 and TargetLynx 2.7 (waters®).

The determination of MG and MG derived AGEs by stable isotopic dilution analysis via LC-MS/MS was described previously (27, 29).

Determination of reactive oxygen, superoxide and nitric oxide species—Determination was based upon analysis via flow cytometry/FACS. All incubation and washing steps of living cells were done in Krebs Ringer HEPES buffer (KRH) including 136 mM NaCl, 4.7mM KCl, 1.25mM CaCl₂, 1.25mM MgSO₄, 10mM HEPES, 0.1% Fatty Acid Free BSA; pH7.4. Treated and untreated cells were stained with Hoechst 33258 NucBlue® (Thermo) for the detection of viable cells. Determination of superoxide production and reactive oxygen species was achieved incubating Schwann cells with MitoSOX™ Red (10 μ M in KRH buffer) and CM-H₂DCFDA (5 μ M in KRH buffer) for 30 min under reduced light conditions. For the determination of nitric oxide species we used 4-Amino-5-Methylamino-2',7'-Difluorofluorescein Diacetate (DAF-FM; 5 μ M in KRH buffer) (all reagents from Thermo). After 2 washing steps, cells were trypsinized and resuspended in 1 ml FACS-Buffer (10% FCS, 1 mM EDTA in PBS). Analysis of fluorophores was performed using a LSRII flow cytometer (BD Biosciences) by gating initial cell population via forward scatter against side scatter signals and detecting viable cells (Hoechst positive) by violet laser (Excitation: 405 nm; Filter: 450/40 nm). Hoechst positive cells

were then analyzed for MitoSOX™ Red by blue laser (Excitation: 488 nm; Filter: 575/26 nm), CM-H₂DCFDA and DAF-FM also by blue laser (Excitation: 488 nm; Filter: 530/30 nm).

Statistical analysis—All data are expressed as mean values ± standard error (SE) and were analyzed for significance using two-

tailed unpaired t-test with Welch's correction. The comparison of more than one group was achieved using an ordinary one-way or two-way ANOVA analysis followed by comparing all groups using *Tukey's* (one-way ANOVA) or *Sidak's* (two-way ANOVA) multiple comparison test. Differences were considered significant at $p < 0.05$.

Acknowledgements: We thank Deutsche Forschungsgemeinschaft (SFB1118 & GRK 1874-DIAMICOM) and DietmarHopp foundation for supporting this study. The authors would also like to thank Barbro Beijer and Prof. Walter Mier from the Department of Nuclear Medicine, University of Heidelberg, for the synthesis of d4-MG and Dr. Karel Klika from the German Cancer Research Center (DKFZ) for the NMR analysis. We also thank members of the Nawroth/Fleming laboratory for helpful comments and discussions.

Conflict of interest: The authors declare that they have no conflicts of interest with the contents of this article.

Author contribution: JM performed and analyzed most of the experiments and wrote the manuscript. TF assisted in experimental preparation and in analysis or interpretation of data. DS and MF assisted in research design and performed initial experiments for the establishment of GLO1 knock-out. VE assisted performing experiments with flow cytometry/fluorescence activated cell sorting (FACS). PN and SH elaborated the idea of this project and assisted in writing the manuscript. All authors reviewed the results and approved the final version of the manuscript.

REFERENCES

1. Goh, S.-Y., and Cooper, M.E. (2008) The Role of Advanced Glycation End Products in Progression and Complications of Diabetes. *J. Clin. Endocrinol. Metab.* **93**, 1143–1152
2. Singh, R., Barden A., Mori T., and Beilin L. (2001) Advanced glycation end-products: a review. *Diabetologia* **44**, 129–146
3. Thornalley, P. J., Langborg, A., and Minhas, H. S. (1999) Formation of glyoxal, methylglyoxal and 3-deoxyglucosone in the glycation of proteins by glucose. *Biochem. J.* **344**, 109–116
4. Phillips S. A., Mirrlees D. and Thornalley P. J. (1993) Modification of the glyoxalase system in streptozotocin-induced diabetic rats: effect of the aldose reductase inhibitor Statil. *Biochem. Pharmacol.* **46**, 805-811
5. Han, Y., Randell, E., Vasdev, S., Gill, V., Gadag, V., Newhook, L.A., Grant, M., and Hagerty, D. (2007) Plasma methylglyoxal and glyoxal are elevated and related to early membrane alteration in young, complication-free patients with type 1 diabetes. *Mol. Cell. Biochem.* **305**, 123-131
6. McLellan, A.C., Thornalley, P.J., Benn, J., and Sonksen, P.H. (1994) Glyoxalase system in clinical diabetes mellitus and correlation with diabetic complications. *Clin. Sci. (Lond.)* **87**, 21-29
7. Allaman, I., Bélanger, M., and Magistretti, P.J. (2015) Methylglyoxal, the dark side of glycolysis. *Front. Neurosci.* **9**, 23
8. Thornalley, P.J. (1990) The glyoxalase system: new developments towards functional characterization of a metabolic pathway fundamental to biological life. *Biochem. J.* **269**, 1-11
9. Thornalley, P.J. (2003) Glyoxalase I—Structure, function and a critical role in the enzymatic defence against glycation. *Biochem. Soc. Trans.* **31**, 1343-1348
10. Skapare, E., Konrade, I., Liepinsh, E., Strele I., Makrecka, M., Bierhaus, A., Lejnieks, A., Pirags, V., and Dambrova, M. (2013) Association of reduced glyoxalase 1 activity and painful peripheral diabetic neuropathy in type 1 and 2 diabetes mellitus patients. *J. Diabetes Complications* **27**, 262-267
11. Jack, M.M., Ryals J.M., and Wright D.E. (2011) Characterisation of glyoxalase 1 in a streptozotocin-induced mouse model of diabetes with painful and insensate neuropathy. *Diabetologia* **54**, 2174-2182
12. Vander Jagt, D.L., and Hunsaker, L.A. (2003) Methylglyoxal metabolism and diabetic complications: Role of aldose reductase, glyoxalase-I, betaine aldehyde dehydrogenase and 2-oxoaldehyde dehydrogenase. *Chem. Biol. Interact.* **143-144**, 341-351
13. Vander Jagt, D.L., Robinson B., Taylor, K.K., and Hunsaker L.L. (1992) Reduction of trioses by NADPH-dependent aldo-keto reductase. *J. Biol. Chem.* **267**, 4364-4369
14. Baba, S.P., Barski, O.A., Ahmed, Y., O'Toole, T.E., Conklin, D.J., Bhatnagar, A., and Srivastava, S. (2009) Reductive metabolism of AGE precursors: a metabolic route for preventing AGE accumulation in cardiovascular tissue. *Diabetes* **58**, 2486-2497
15. Izaguirre, G., Kikonyogo, A., and Pietruszko, R. (1998) Methylglyoxal as substrate and inhibitor of human aldehyde dehydrogenase: comparison of kinetic properties among the three isozymes. *Comp. Biochem. Physiol.* **119B**, 747-754
16. Lee, J.Y., Song, J., Kwon, K., Jang, S., Kim, C., Baek, K., Kim, J., and Park, C. (2012) Human DJ-1 and its homologs are novel glyoxalases. *Hum. Mol. Genet.* **21**, 3215-3225
17. Brouwers, O., Niessen, P.M., Ferreira, I., Miyata, T., Scheffer, P.G., Teerlink, T., Schrauwen, P., Brownlee, M., Stehouwer, C.D., and Schalkwijk, C.G. (2011) Overexpression of glyoxalase-I reduces hyperglycemia-induced levels of advanced glycation end products and oxidative stress in diabetic rats. *J. Biol. Chem.* **286**, 1374-1380
18. Bierhaus, A., Fleming, T., Stoyanov, S., Leffler, A., Babes, A., Neacsu, C., Sauer, S.K., Eberhardt, M., Schnolzer, M., Lasischka, F., Neuhuber, W.L., Kichko, T.I., Konrade, I., Elvert, R., Mier, W., Pirags, V., Lukic, I.K., Morcos, M., Dehmer, T., Rabbani, N., Thornalley, P.J., Edelstein, D., Nau, C., Forbes, J., Humpert, P.M., Schwaninger, M., Ziegler, D., Stern, D.M.,

- Cooper, M.E., Haberkorn, U., Brownlee, M., Reeh, P.W., Nawroth, P.P. (2012) Methylglyoxal modification of Na(v)1.8 facilitates nociceptive neuron firing and causes hyperalgesia in diabetic neuropathy. *Nat. Med.* **18**, 926-933
19. Shinohara, M., Thornalley, P. J., Giardino, I., Beisswenger, P., Thorpe, S. R., Onorato, J., and Brownlee, M. (1998) Overexpression of glyoxalase-I in bovine endothelial cells inhibits intracellular advanced glycation endproduct formation and prevents hyperglycemia-induced increases in macromolecular endocytosis. *J. Clin. Invest.* **101**, 1142–1147
 20. Barski, O. A., Tipparaju, S. M., and Bhatnagar, A. (2008) The Aldo-Keto Reductase Superfamily and its Role in Drug Metabolism and Detoxification. *Drug Metabolism Reviews.* **40**, 553–624
 21. Giacco, F., Du, X., D'Agati, V. D., Milne, R., Sui, G., Geoffrion, M., and Brownlee, M. (2014) Knockdown of glyoxalase 1 mimics diabetic nephropathy in nondiabetic mice. *Diabetes.* **63**, 291–299
 22. Xue, M., Rabbani, N., Momiji, H., Imbasi, P., Anwar, M. M., Kitteringham, N., Park, B. K., Souma, T., Moriguchi, T., Yamamoto, M., and Thornalley, P. J. (2012) Transcriptional control of glyoxalase 1 by Nrf2 provides a stress-responsive defence against dicarbonyl glycation. *Biochem. J.* **443**, 213–222
 23. Vander Jagt, D. L., Hassebrook, R. K., Hunsaker, L. A., Brown, W. M., and Royer, R. E. (2001) Metabolism of the 2-oxoaldehyde methylglyoxal by aldose reductase and by glyoxalase-I: roles for glutathione in both enzymes and implications for diabetic complications. *Chemico-Biological Interactions.* **130-132**, 549–562
 24. Rae, C., Berners-Price, S.J., Bulliman, B.T., and Kuchel, P.W. (1990) Kinetic analysis of the human erythrocyte glyoxalase system using ¹H NMR and a computer model. *Eur. J. Biochem.* **193**, 83-90
 25. Vander Jagt, D.L., Dolphin, D., Paulson, R., and Avramovic, O. (1989) The glyoxalase system, in glutathione: chemical, biochemical, and medical aspects. *Wiley and Sons.* **Part A**, 598-641
 26. Beilin, E., Baker, L. J., Culbert, P., and Toltl, N. P. (2008) Quantitation of acetol in common pharmaceutical excipients using LC-MS. *J. Pharm. Biomed. Anal.* **46**, 316–321
 27. Rabbani, N., and Thornalley, P. J. (2014) Measurement of methylglyoxal by stable isotopic dilution analysis LC-MS/MS with corroborative prediction in physiological samples. *Nat. Protoc.* **9**, 1969–1979
 28. Denizot, F., and Lang, R. (1986) Rapid colorimetric assay for cell growth and survival. Modifications to the tetrazolium dye procedure giving improved sensitivity and reliability. *J. Immunol. Methods.* **89**, 271–277
 29. Thornalley, P. J., and Rabbani, N. (2014) Detection of oxidized and glycated proteins in clinical samples using mass spectrometry — A user's perspective. *BBA-Gen. Subjects* **1840**, 818–829
 30. Rahman, I., Kode, A., and Biswas, S. K. (2007) Assay for quantitative determination of glutathione and glutathione disulfide levels using enzymatic recycling method. *Nat. Protoc.* **1**, 3159–3165
 31. Bradford, M. M. (1976) A rapid and sensitive method for the quantitation of microgram quantities of protein utilizing the principle of protein-dye binding. *Anal. Biochem.* **72**, 248–254
 32. McLellan, A. C., and Thornalley, P. J. (1989) Glyoxalase activity in human red blood cells fractionated by age. *Mech. Ageing Dev.* **48**, 63–71
 33. Srivastava, S., Watowich, S. J., Petrash, J. M., Srivastava, S. K., and Bhatnagar, A. (1999) Structural and Kinetic Determinants of Aldehyde Reduction by Aldose Reductase. *Biochemistry* **38**, 42–54
 34. Goedhart, J., von Stetten, D., Noirclerc-Savoye, M., Lelimosin, M., Joosen, L., Hink, M. A., van Weeren, L., Gadella, T. W. J., and Royant, A. (2012) Structure-guided evolution of cyan fluorescent proteins towards a quantum yield of 93%. *Nat. Commun.* **3**, 751
 35. Rabbani, N., and Thornalley, P. J. (2014) The Critical Role of Methylglyoxal and Glyoxalase 1 in Diabetic Nephropathy. *Diabetes* **63**, 50–52
 36. Kaiserova, K., Tang, X.-L., Srivastava, S., and Bhatnagar, A. (2008) Role of Nitric Oxide in Regulating Aldose Reductase Activation in the Ischemic Heart. *J. Biol. Chem.* **283**, 9101–9112

37. Baba, S. P., Wetzelberger, K., Hoetker, J. D., and Bhatnagar, A. (2009) Posttranslational glutathiolation of aldose reductase (AKR1B1): A possible mechanism of protein recovery from S-nitrosylation. *Chem.-Biol. Interactions* **178**, 250–258
38. Brownlee, M. (2001) Biochemistry and molecular cell biology of diabetic complications. *Nature* **414**, 813–820
39. Mizisin, A. P. (2014) Mechanisms of diabetic neuropathy. in *Handbook of Clinical Neurology*, Elsevier, **126**, 401–428
40. Kern, T. S., and Engerman, R. L. (1982) Immunohistochemical distribution of aldose reductase. *Histochem. J.* **14**, 507–515
41. Utsunomiya, K. (2014) Physiological and Pathological Roles of Aldose Reductase in Schwann Cells. *J. Mol. Genet. Med.* **S1**, 012
42. Schemmel, K. E., Padiyara, R. S., and D'Souza, J. J. (2010) Aldose reductase inhibitors in the treatment of diabetic peripheral neuropathy: a review. *J. Diabetes Complications* **24**, 354–360
43. Ramirez, M. A., and Borja, N. L. (2008) Epalrestat: An Aldose Reductase Inhibitor for the Treatment of Diabetic Neuropathy. *Pharmacotherapy* **28**, 646–655
44. Hu, X., Li, S., Yang, G., Liu, H., Boden, G., and Li, L. (2014) Efficacy and Safety of Aldose Reductase Inhibitor for the Treatment of Diabetic Cardiovascular Autonomic Neuropathy: Systematic Review and Meta-Analysis. *PLoS ONE* **9**, e87096
45. Qu, Z., Meng, F., Bomgarden, R. D., Viner, R. I., Li, J., Rogers, J. C., Cheng, J., Greenleaf, C. M., Cui, J., Lubahn, D. B., Sun, G. Y., and Gu, Z. (2014) Proteomic Quantification and Site-Mapping of S -Nitrosylated Proteins Using Isobaric iodoTMT Reagents. *J. Proteome Res.* **13**, 3200–3211
46. Belanger, M., Yang, J., Petit, J.-M., Laroche, T., Magistretti, P. J., and Allaman, I. (2011) Role of the Glyoxalase System in Astrocyte-Mediated Neuroprotection. *J. Neurosci.* **31**, 18338–18352
47. Thornalley, P. J. (1993) The glyoxalase system in health and disease. *Mol. Aspects Med.* **14**, 287–371
48. Xue, M., Weickert, M. O., Qureshi, S., Kandala, N.-B., Anwar, A., Waldron, M., Shafie, A., Messenger, D., Fowler, M., Jenkins, G., Rabbani, N., and Thornalley, P. J. (2016) Improved Glycemic Control and Vascular Function in Overweight and Obese Subjects by Glyoxalase 1 Inducer Formulation. *Diabetes* **65**, 2282–2294
49. Freeman, O. J., Unwin, R. D., Dowsey, A. W., Begley, P., Ali, S., Hollywood, K. A., Rustogi, N., Petersen, R. S., Dunn, W. B., Cooper, G. J. S., and Gardiner, N. J. (2015) Metabolic dysfunction is restricted to the sciatic nerve in experimental diabetic neuropathy. *Diabetes* **65**, 228–238
50. Viader, A., Sasaki, Y., Kim, S., Strickland, A., Workman, C. S., Yang, K., Gross, R. W., and Milbrandt, J. (2013) Aberrant Schwann Cell Lipid Metabolism Linked to Mitochondrial Deficits Leads to Axon Degeneration and Neuropathy. *Neuron*. **77**, 886–898
51. Thornalley, P. J., Battah, S., Ahmed, N., Karachalias, N., Agalou, S., Babaei-Jadidi, R., and Dawnay, A. (2003) Quantitative screening of advanced glycation endproducts in cellular and extracellular proteins by tandem mass spectrometry. *Biochem. J.* **375**, 581–592
52. Hidmark, A., Fleming, T., Vittas, S., Mendler, M., Deshpande, D., Groener, J. B., Müller, B. P., Reeh, P. W., Sauer, S. K., Pham, M., Muckenthaler, M. U., Bendszus, M., and Nawroth, P. P. (2014) A new paradigm to understand and treat diabetic neuropathy. *Exp. Clin. Endocrinol. Diabetes.* **122**, 201–207
53. Clelland, J. D., and Thornalley, P. J. (1990) Synthesis of 14C-labelled methylglyoxal and S-D-lactoylglutathione. *J. Labelled Comp. Radiopharm.* **28**, 1455–1464
54. Wang, T., Kartika, R., and Spiegel, D. A. (2012) Exploring Post-translational Arginine Modification Using Chemically Synthesized Methylglyoxal Hydroimidazolones. *J. Am. Chem. Soc.* **134**, 8958–8967
55. Ahmed, N., Dobler, D., Dean, M., and Thornalley, P. J. (2005) Peptide mapping identifies hotspot site of modification in human serum albumin by methylglyoxal involved in ligand binding and esterase activity. *J. Biol. Chem.* **280**, 5724–5732

56. Peters, A. S., Lercher, M., Fleming, T. H., Nawroth, P. P., Bischoff, M. S., Dihlmann, S., Böckler, D., and Hakimi, M. (2016) Reduced glyoxalase 1 activity in carotid artery plaques of nondiabetic patients with increased hemoglobin A1c level. *J. Vasc. Surg.* 10.1016/j.jvs.2016.04.025
57. Kwon, N. S., Lee, S. H., Choi, C. S., Kho, T., and Lee, H. S. (1994) Nitric oxide generation from streptozotocin. *FASEB J.* **8**, 529–533
58. Carlberg, I., and Mannervik, B. (1985) Glutathione reductase. *Meth. Enzymol.* **113**, 484–490
59. Livak, K. J., and Schmittgen, T. D. (2001) Analysis of Relative Gene Expression Data Using Real-Time Quantitative PCR and the 2- $\Delta\Delta$ CT Method. *Methods.* **25**, 402–408
60. Su, Y., Qadri, S. M., Wu, L., and Liu, L. (2013) Methylglyoxal modulates endothelial nitric oxide synthase-associated functions in EA.hy926 endothelial cells. *Cardiovascular Diabetology.* **12**, 134
61. Turkseven, S., Ertuna, E., Yetik-Anacak, G., and Yasa, M. (2014) Methylglyoxal causes endothelial dysfunction: the role of endothelial nitric oxide synthase and AMP-activated protein kinase α . *J Basic Clin Physiol and Pharmacol.* **25**, 109-115
62. Chang, T., Wang, R., and Wu, L. (2005) Methylglyoxal-induced nitric oxide and peroxynitrite production in vascular smooth muscle cells. *Free Radic. Biol. Med.* **38**, 286–293

FOOTNOTES

This work was supported in whole or part by Deutsche Forschungsgemeinschaft (SFB1118)

The abbreviations used are: 1400 W dihydrochloride, N-([3-(Aminomethyl)phenyl]methyl)-ethanimidamide dihydrochloride; 2-AAPA, R,R'-2-Acetylamino-3-[4-(2-acetylamino-2-carboxyethyl-sulfanylthiocarbonylamino)phenylthio-carbamoylsulfanyl]propionic acid hydrate; AGE, advanced glycation endproduct; AKR, aldo-keto reductase; ALDH, aldehyde dehydrogenase; GLO1, glyoxalase 1; HTA, hemithioacetate; KRH, Krebs Ringer HEPES buffer; MG, methylglyoxal; MG-H1, methylglyoxal-derived hydroimidazolone 1; PFBHA, O-(2,3,4,5,6-pentafluorophenyl)methyl hydroxylamin

TABLES

TABLE1. GLO1-activity of wild-type Schwann cells and 3 individual GLO1^{-/-} Schwann cell clones. Activity is described in units (U), where 1 U is the amount of GLO1 which catalyzes the formation of 1 μ mol of S-D-lactoylglutathione per minute. Values are the mean of at least 3 independent experiments \pm standard error.

FIGURE LEGENDS

FIGURE 1. Loss of GLO1 is not associated with increased Levels of MG or MG-specific AGEs.

A, representative western blot analysis of total cell extracts (30 μ g of protein) from Schwann cells (wild-type & 3 GLO1^{-/-} clones; in brackets: passage number after subculturing) probed with anti-GLO1 antibody and anti- β -Actin antibody as a loading control. B, intracellular MG-levels in wild-type Schwann cells and 3 individual GLO1^{-/-} Schwann cell clones cultured under baseline conditions (5mM Glucose). C, densitometry analysis and representative western blot of total cell extracts (30 μ g of protein) from Schwann cells (wild-type & 3 GLO1^{-/-} clones) probed with anti-MG-H1 (Methylglyoxal-derived hydroimidazolone) antibody detecting MG modified arginine residues and anti- β -Actin antibody as a loading control. D, intracellular AGE-levels of MG modified arginine (MG-H1) and lysine (N-epsilon-(carboxyethyl)lysine; CEL) residues after exhaustive enzymatic digestion and determination via LC-MS/MS. Values are the mean of at least 3 independent experiments \pm standard error. Western blot bar graphs represent the mean of 3 independent experiments \pm standard error.

FIGURE 2. Several types of Oxidoreductases are potentially involved in the detoxification of MG in GLO1^{-/-} Schwann cells. A, baseline mRNA expression of different subtypes of aldo-keto reductase (AKR) and aldehyde-dehydrogenase (ALDH) in wild-type Schwann cells (□) and 3 individual GLO1^{-/-} Schwann cell clones (■). Values for wild-type cells are standardized to 100%. B, mRNA expression of different subtypes of aldo-keto reductase (AKR) and aldehyde dehydrogenase (ALDH) in 3 different GLO1^{-/-} Schwann cell clones with (■) and without (□) MG-treatment (50 μM; 6h). C, mRNA expression of different subtypes of aldo-keto reductase (AKR) and aldehyde dehydrogenase (ALDH) in wild-type Schwann cells with (■) and without (□) MG-treatment (50 μM; 6h). All data are normalized to β-Actin and represent the mean of at least 3 independent experiments ± standard error.

FIGURE 3. Aldo-keto reductases contribute to the efficient detoxification of hemithioacetal. A, kinetic profile of the aldo-keto reductases (AKR (□)) & aldehyde dehydrogenases (ALDH (●)) catalyzed reduction of MG in the cytosol of GLO1^{-/-} Schwann cells. B, kinetic profile of the aldo-keto reductases (AKR) catalyzed reduction of MG in wild-type (●) and GLO1^{-/-} (□) Schwann cells. C, kinetic profile of the aldo-keto reductases (AKR) catalyzed reduction of HTA in wild-type (●) Schwann cells and 3 individual GLO1^{-/-} (□) Schwann cell clones. AKR: V_{max} [μmol NADPH/min/mg protein]; K_m [mM]; ALDH: V_{max} [μmol NADH/min/mg protein]; K_m [mM]; D, densitometry analysis and representative western blot of total cell extracts (30 μg of protein) from Schwann cells (wild-type & 3 GLO1^{-/-} clones) probed with anti-AKR1b3 antibody and anti-β-Actin antibody as a loading control. All kinetic data represent the mean of at least 4 independent experiments ± standard error. Western blot bar graphs represent the mean of 3 independent experiments ± standard error.

FIGURE 4. S-Nitrosylation of AKR1b3 is beneficial for the efficient detoxification of dicarbonyl species in GLO1^{-/-} Schwann cells. A, intracellular levels of nitric oxide species in wild-type (□) Schwann cells and 3 individual GLO1^{-/-} (■) Schwann cell clones using flow cytometry and DAF-FM as a dye reagent. B, enzymatic activity of nitric oxide synthases in wild-type and GLO1^{-/-} Schwann cells (clone 1), where 1 unit of NOS activity is the amount of enzyme required to yield 1 μmol of nitric oxide/min. C, densitometry analysis and representative western blot of whole cell lysates of wild-type Schwann cells and 3 individual GLO1^{-/-} Schwann cell clones with & without MG-treatment (50 μM; 6h) detecting nitrosylated cystein residues using IodoTMT switch technique. Lysates were probed with anti-IodoTMT and β-Actin as a loading control. D, baseline mRNA expression of the 3 different subtypes of nitric oxide synthases (NOS) in wild-type (□) Schwann cells and 3 individual GLO1^{-/-} (■) Schwann cell clones. Values for NOS1 in wild-type Schwann cells were standardized to 100%. E, intracellular MG-levels in wild-type Schwann cells and 3 individual GLO1^{-/-} Schwann cell clones treated with iNOS inhibitor 1400W dihydrochloride (100 μM; 24h). F, median lethal dose (LD₅₀) for MG (48h exposure time) in wild-type and GLO1^{-/-} Schwann cells (clone 1) treated with iNOS inhibitor 1400 W dihydrochloride (100 μM). G, densitometry analysis and representative western blot of total cell extracts (30 μg of protein) from wild-type Schwann cells and 3 individual GLO1^{-/-} Schwann cell clones with & without 1400W-treatment (100 μM; 24h), probed with anti-MG-H1 (Methylglyoxal-derived hydroimidazolone) antibody detecting MG modified arginine residues and anti-β-Actin antibody as a loading control. H, densitometry analysis and representative western blot of recombinant AKR1b3 protein with and without exposure to a nitric oxide donor (STZ). Blots were probed with anti-AKR1b3 antibody and stained with Ponceau S staining as a loading control. I, enzymatic activity assay of recombinant AKR1b3 under substrate saturating conditions (2 mM of each) with (■) and without (□) the exposure to a NO donor, where 1 unit is the amount of AKR1b3 which catalyzes the formation of 1 μmol of NADP in 1 minute. All data represent the mean of at least 4 independent experiments ± standard error. Western blot bar graphs represent the mean of 3 independent experiments ± standard error.

FIGURE 5. AKR1b3 has an essential role in maintaining cellular viability and preventing MG accumulation, formation of MG modified proteins and oxygen species. A, intracellular MG-levels in wild-type Schwann cells and 3 individual GLO1^{-/-} Schwann cell clones treated with AKR1b3 inhibitor Epalrestat (10 μM; 24h). B, median lethal dose (LD₅₀) for MG (48h exposure time) in wild-type

Schwann cells and 3 individual GLO1^{-/-} Schwann cell clones treated with AKR1b3 inhibitor Epalrestat (10 μM), transfected with siRNA against AKR1b3 or control siRNA (MOCK) and transfected with mammalian expression vector for AKR1b3 (Overexpression - OE). Representative western blots probed with anti-AKR1b3 antibody and anti-β-Actin antibody as a loading control demonstrating the decrease (siRNA) or increase (OE) in AKR1b3 protein expression. All data represent the mean of at least 6 independent experiments ± standard error. C, densitometry analysis and representative western blot of total cell extracts (30 μg of protein) from wild-type Schwann cells and 3 individual GLO1^{-/-} Schwann cell clones with & without Epalrestat-treatment (10 μM; 24h), probed with anti-MG-H1 (Methylglyoxal-derived hydroimidazolone) antibody detecting MG modified arginine residues and anti-β-Actin antibody as a loading control. D, intracellular levels of H₂O₂ or superoxide species in wild-type (WT) and GLO1^{-/-} Schwann cells (clone 1) treated with AKR1b3 inhibitor Epalrestat (10μM; 24h) as determined by flow cytometry. All data represent the mean of at least 4 independent experiments ± standard error. Western blot bar graphs represent the mean of 3 independent experiments ± standard error.

FIGURE 6. GSH reductase is required to preserve cellular GSH concentration in GLO1^{-/-} Schwann cells and to assist in the detoxification of dicarbonyls. A, cytosolic GSH content after the incubation of wild-type (○) Schwann cells or 3 individual GLO1^{-/-} (■) Schwann cell clones with HTA (0.2 mM) for 10, 20, 30, 60, 90 and 120 minutes. The dotted line indicates the time point (0 min) when HTA was added to the cells. B, cytosolic GSSG content after the incubation of wild-type (○) Schwann cells or 3 individual GLO1^{-/-} (■) Schwann cell clones with HTA (0.2 mM) for 10, 20, 30, 60, 90 and 120 minutes. The dotted line indicates the time point (0 min) when HTA was added to the cells. All data represent the mean of at least 3 independent experiments ± standard error. C, densitometry analysis and representative western blot of total cell extracts (30 μg of protein) from Schwann cells (wild-type & 3 GLO1^{-/-} clones) probed with anti-GSH reductase antibody and anti-β-Actin antibody as a loading control. D, enzymatic activity assay of GSH reductase in the cytosol of wild-type (□) Schwann cells or 3 individual GLO1^{-/-} (■) Schwann cell clones under substrate saturating conditions (5 mM GSSG), where 1 unit is the amount of GSH reductase which catalyzes the formation of 1 μmol of NADP in 1 minute. E, cytosolic GSH content in wild-type (□) Schwann cells or 3 individual GLO1^{-/-} (■) Schwann cell clones treated with GSH reductase inhibitor 2-APAA (5μM, 6h). F, cytosolic GSSG content in wild-type (□) Schwann cells or 3 individual GLO1^{-/-} (■) Schwann cell clones treated with GSH reductase inhibitor 2-APAA (5 μM, 6h). G, intracellular MG-levels in wild-type (□) Schwann cells and 3 individual GLO1^{-/-} (■) Schwann cell clones treated with GSH reductase inhibitor 2-APAA (5 μM; 24h). H, median lethal dose (LD₅₀) for MG (48h exposure time) in wild-type and GLO1^{-/-} Schwann cells (clone 1) treated with GSH reductase inhibitor 2-APAA (5 μM). I, densitometry analysis and representative western blot of total cell extracts (30 μg of protein) from wild-type Schwann cells and 3 individual GLO1^{-/-} Schwann cell clones with & without 2-APAA-treatment (5 μM; 24h), probed with anti-MG-H1 (Methylglyoxal-derived hydroimidazolone) antibody detecting MG modified arginine residues and anti-β-Actin antibody as a loading control. J, intracellular levels of H₂O₂ or superoxide species in in wild-type and GLO1^{-/-} Schwann cells (clone 1) treated with GSH reductase inhibitor 2-APAA (10μM; 24h) as determined by flow cytometry. All data represent the mean of at least 4 independent experiments ± standard error. Western blot bar graphs represent the mean of 3 independent experiments ± standard error.

FIGURE 7. Product distribution after *in vivo* conversion of methylglyoxal in GLO1^{-/-} Schwann cells is in the favor of lactaldehyde. A, representative chromatogram of intracellular d4-products in wild-type Schwann cells 60 min after the exposure to d4-MG. Chemical structure displays the complex of labeled d4-D-Lactate/d4-hydroxyacetone and the derivatizing agent (PFBHA) B, representative chromatogram of intracellular d4-products in GLO1^{-/-} Schwann cells 60 min after the exposure to d4-MG. Chemical structure displays the complex of labeled d4-lactaldehyde / d4-hydroxyacetone and the derivatizing agent (PFBHA) C, product distribution of isotopically labeled intracellular metabolites in percent after the conversion of d4-MG *in vivo*. Wild-type and GLO1^{-/-} Schwann cells were exposed to isotopically labeled d4-MG (100 μM) for 60 minutes and products were analyzed by LC-MS/MS.

TABLE 1

Clone # (passage)	GLO1 activity [U/mg Protein]
WT GLO1 ^{+/+} (23)	1.11 ± 0.058
#1 GLO1 ^{-/-} (10)	0.005 ± 0.0012
#2 GLO1 ^{-/-} (10)	0.009 ± 0.0015
#3 GLO1 ^{-/-} (10)	0.008 ± 0.0003

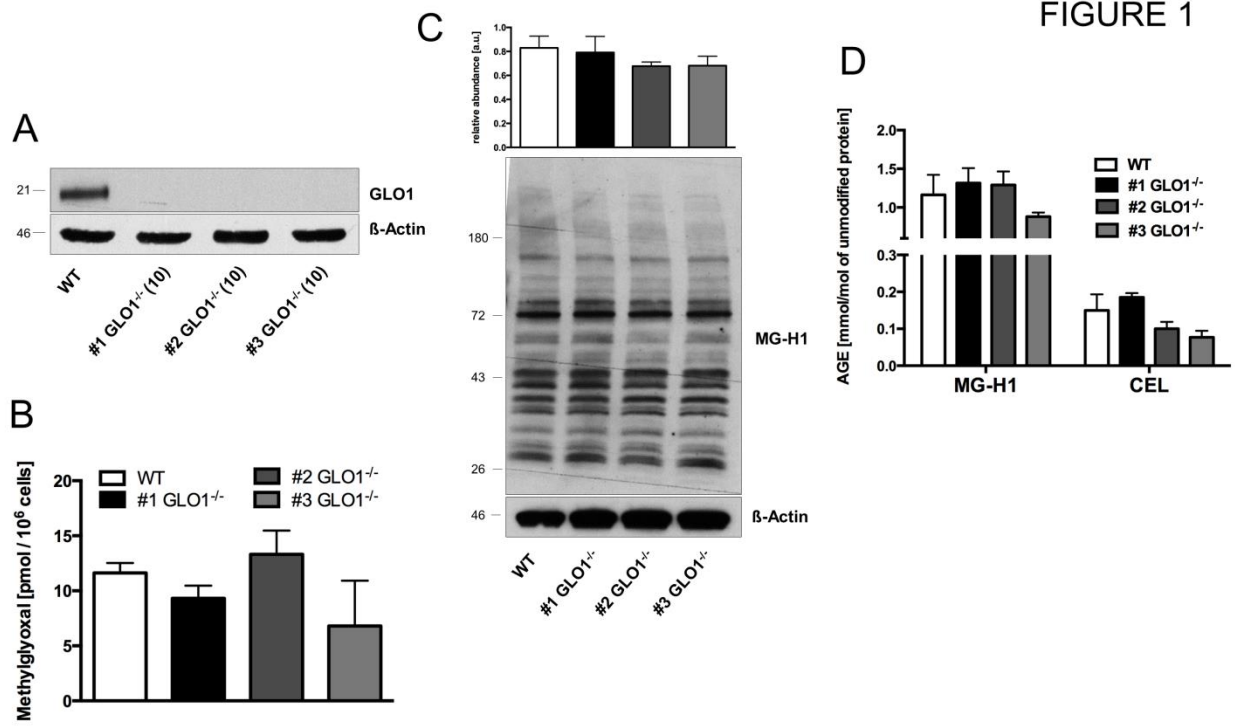


FIGURE 1

FIGURE 2

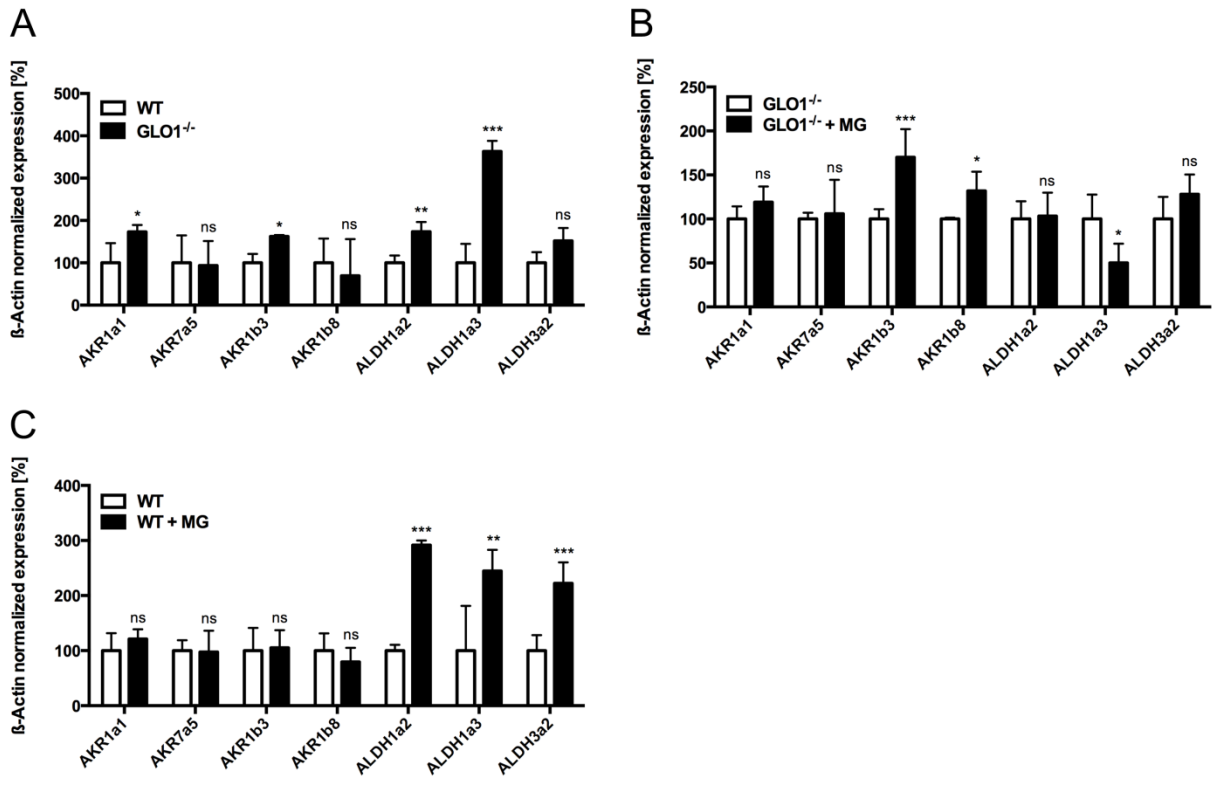


FIGURE 3

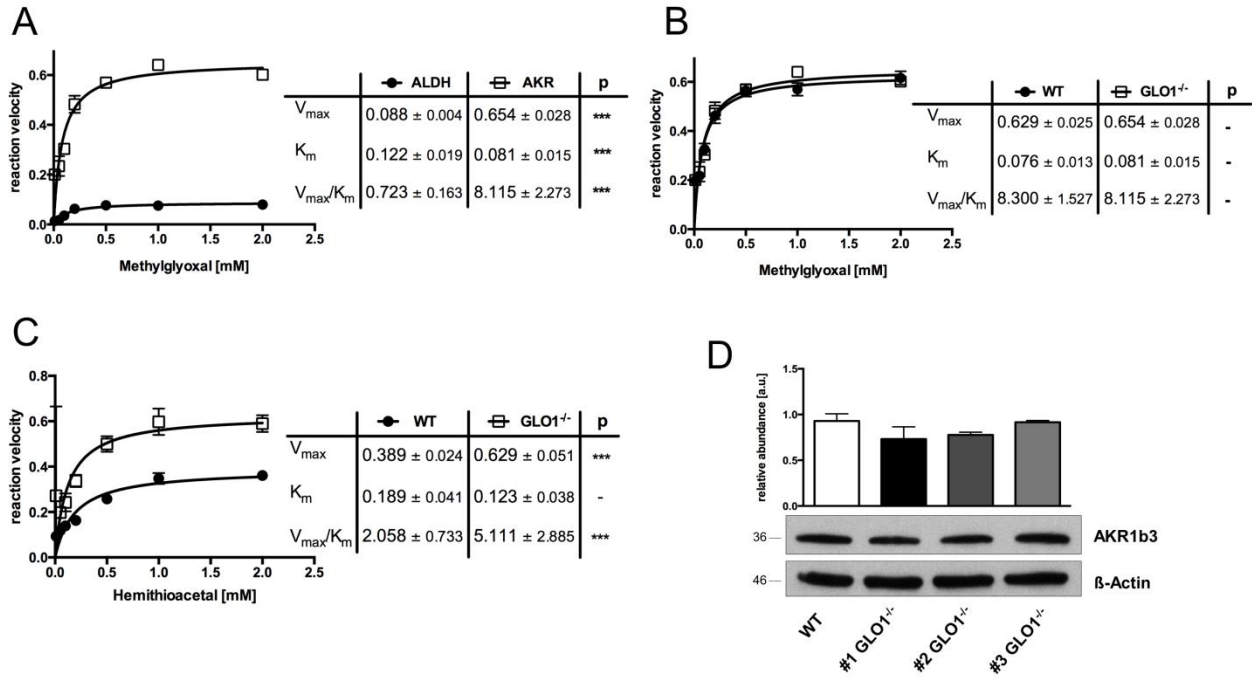


FIGURE 4

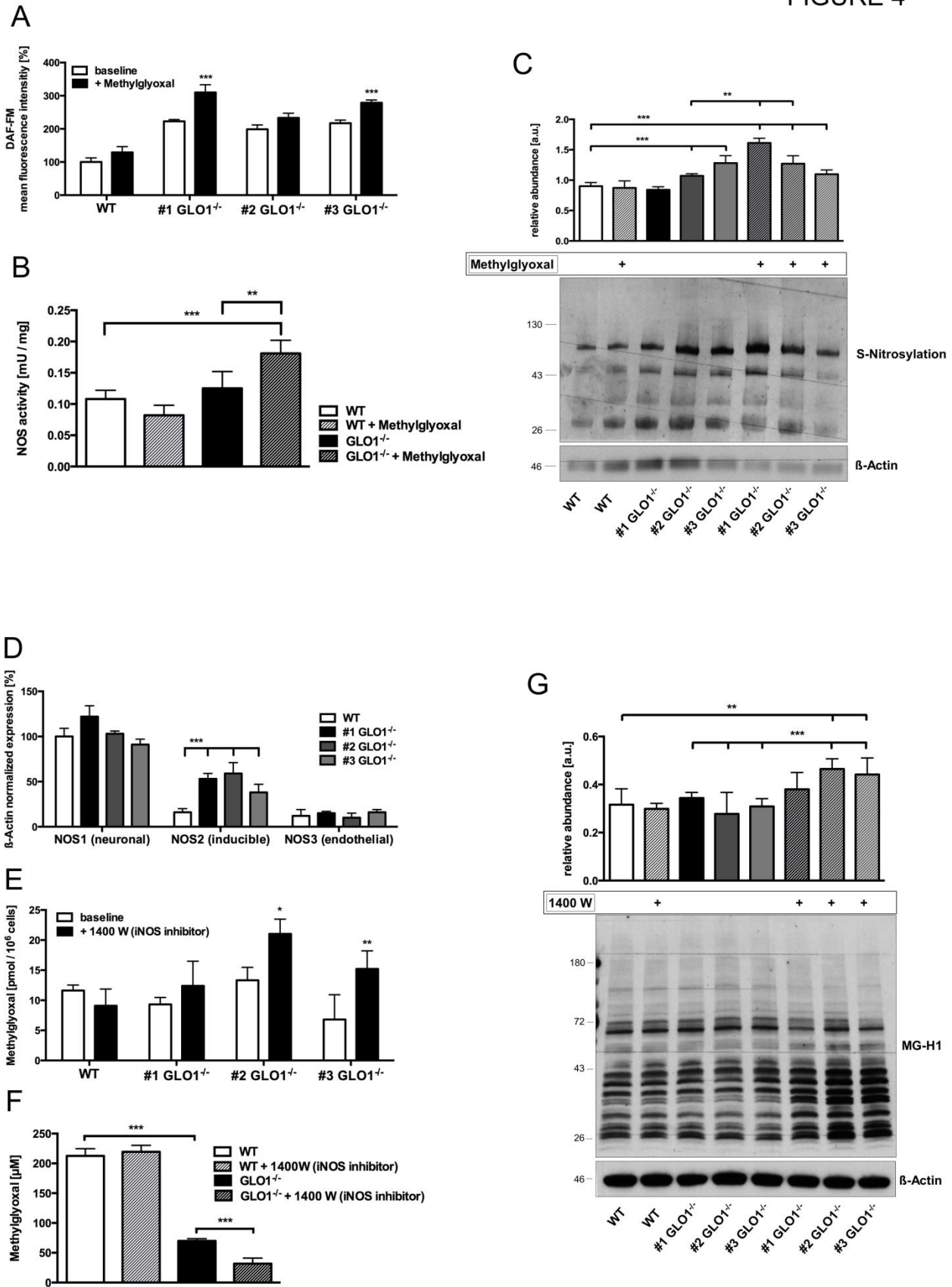


FIGURE 4

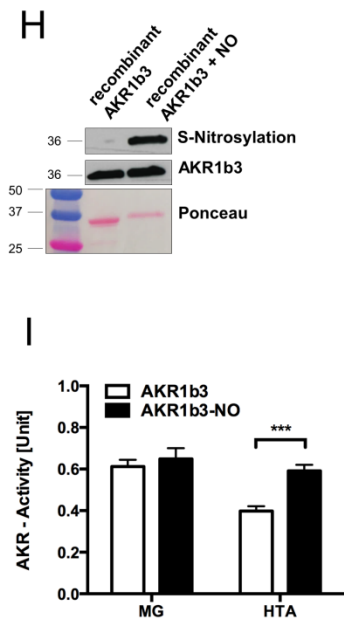
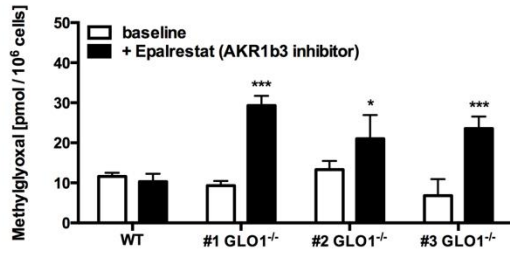
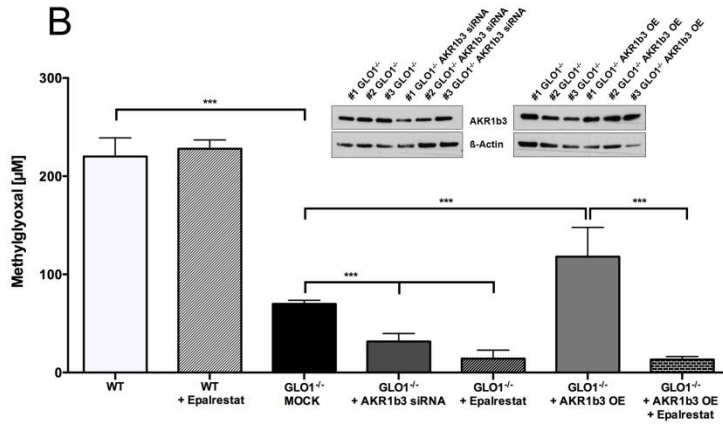


FIGURE 5

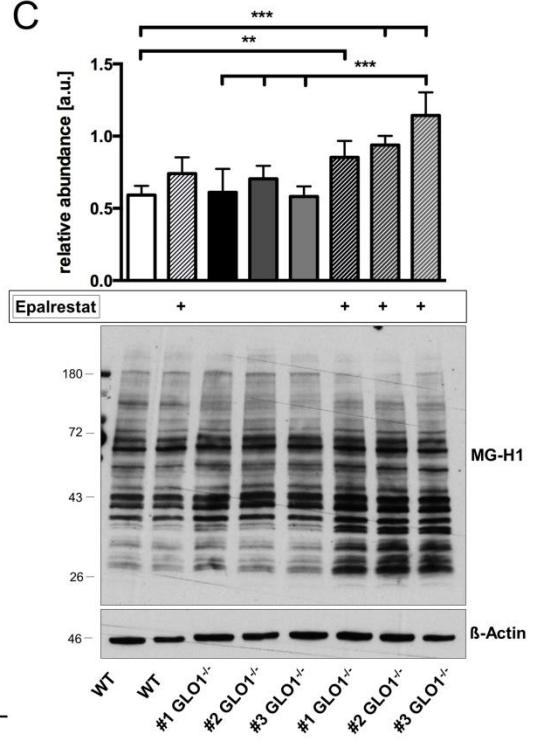
A



B



C



D

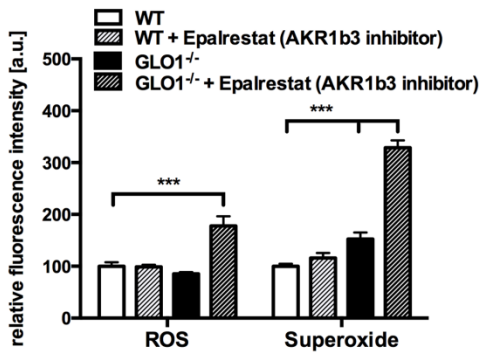


FIGURE 6

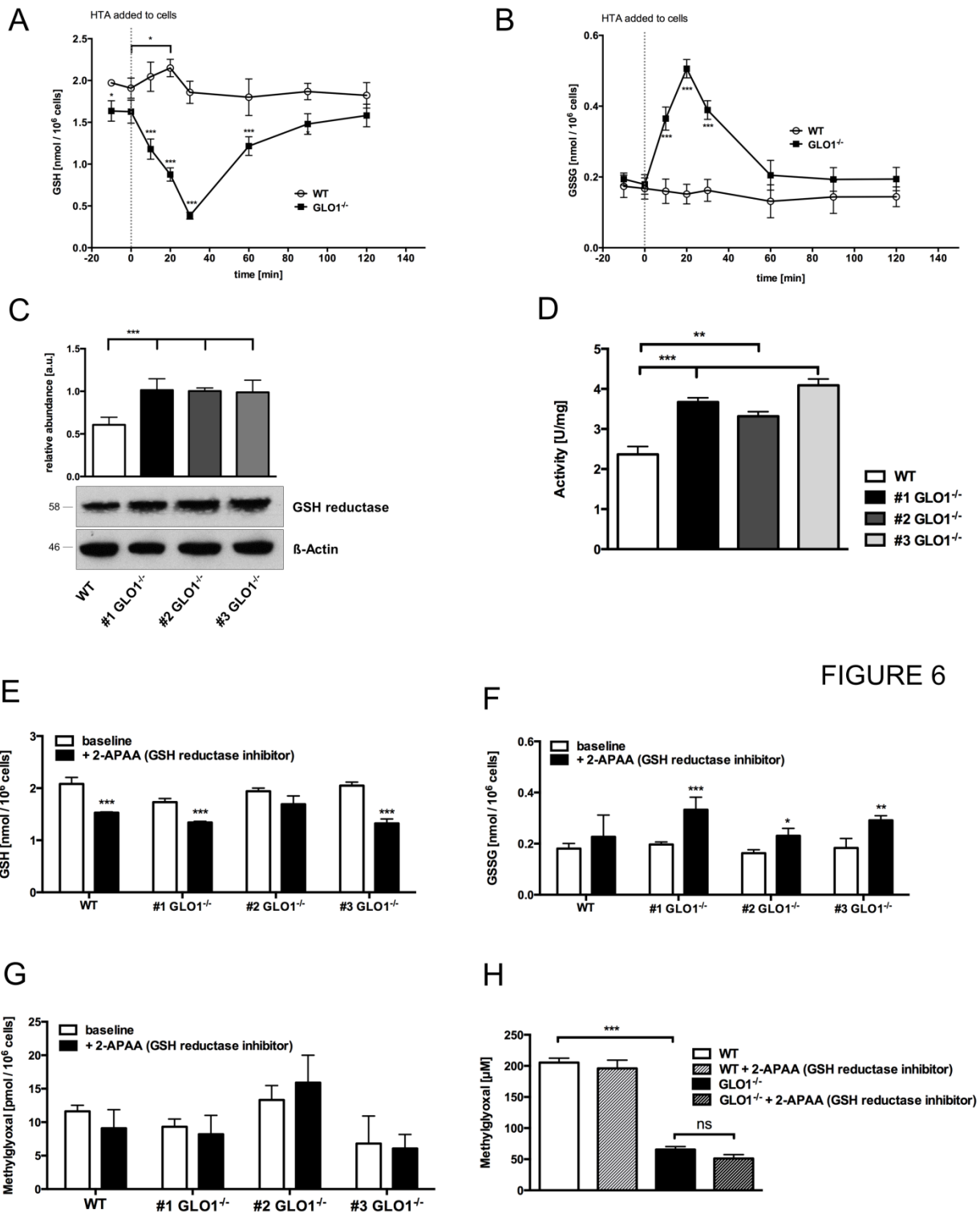


FIGURE 6

FIGURE 6

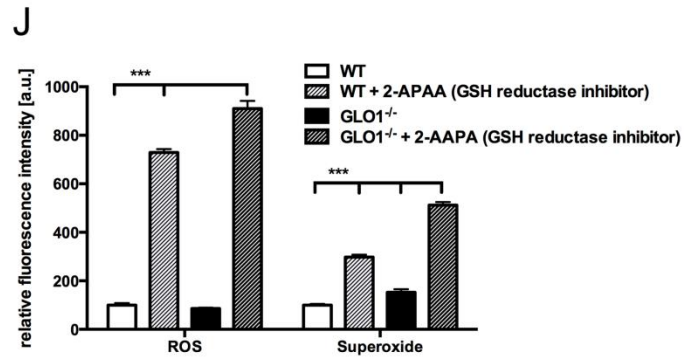
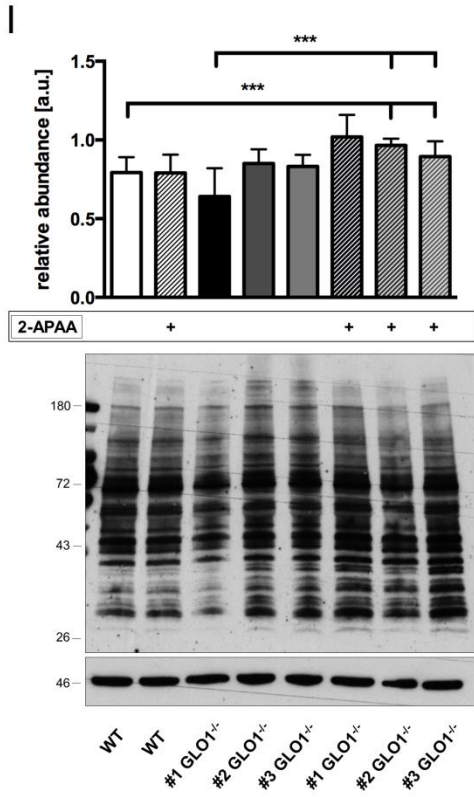
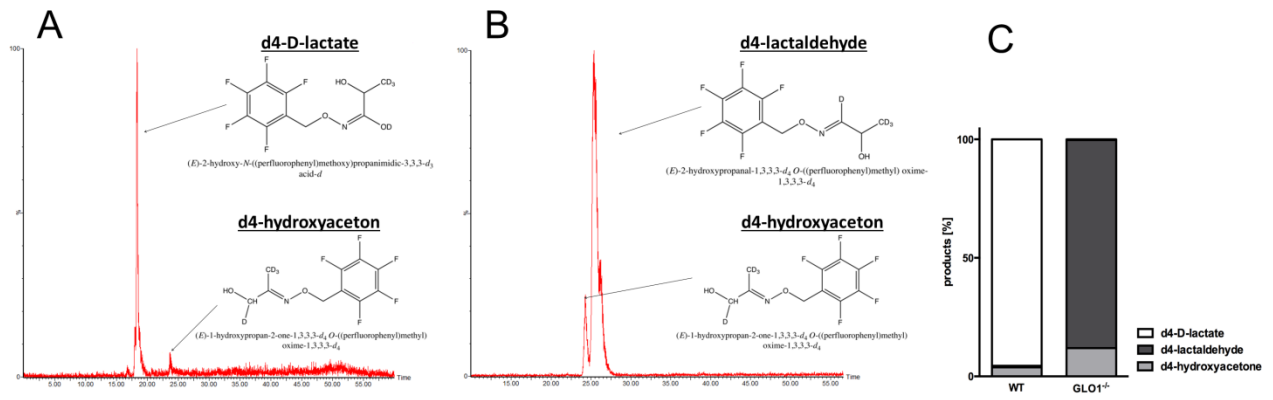


FIGURE 7

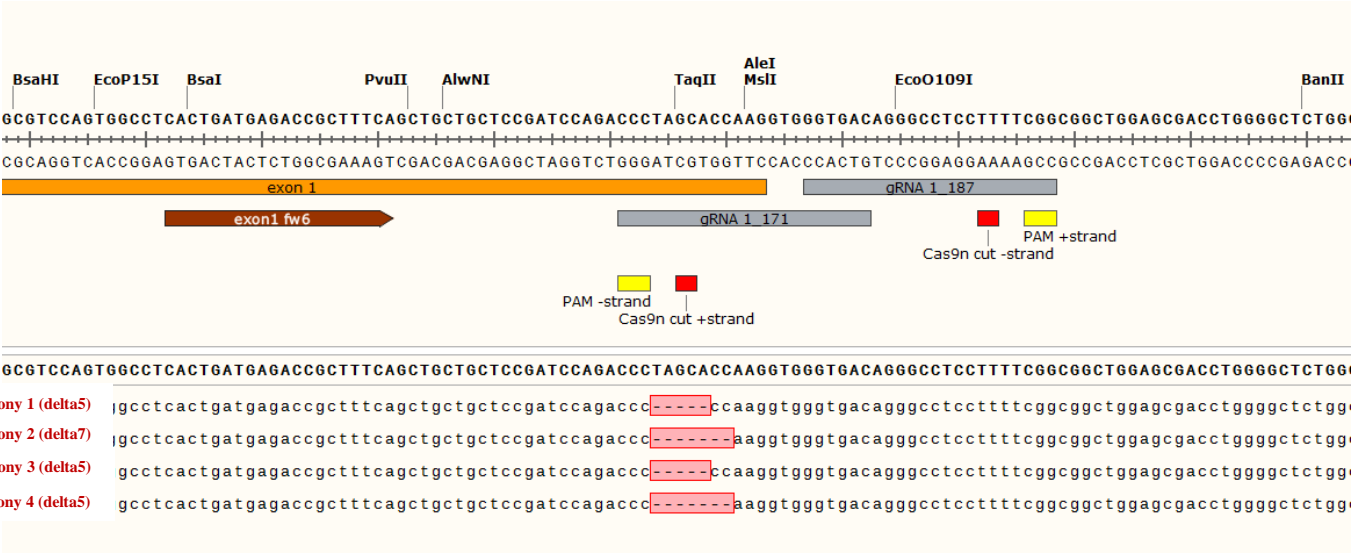


Supplementary data for the manuscript named:

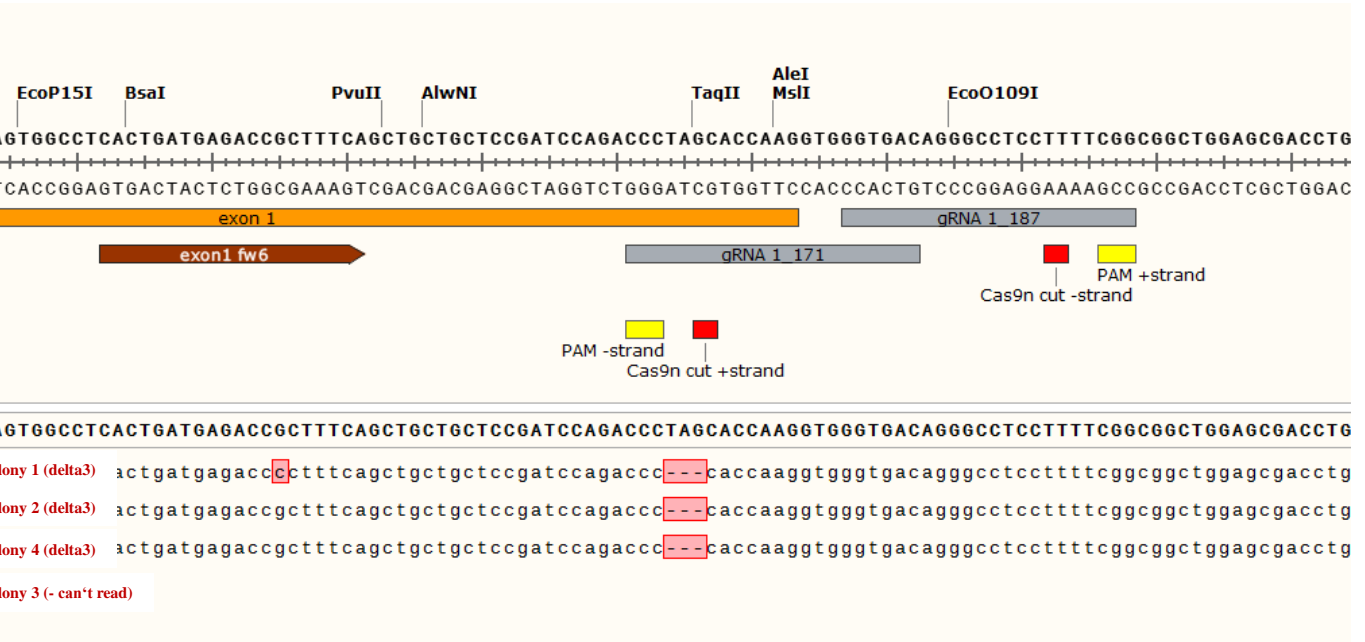
**Loss of Glyoxalase 1 Induces Compensatory Mechanism to Achieve
Dicarbonyl Detoxification in Mammalian Schwann Cells**

Sequencing results

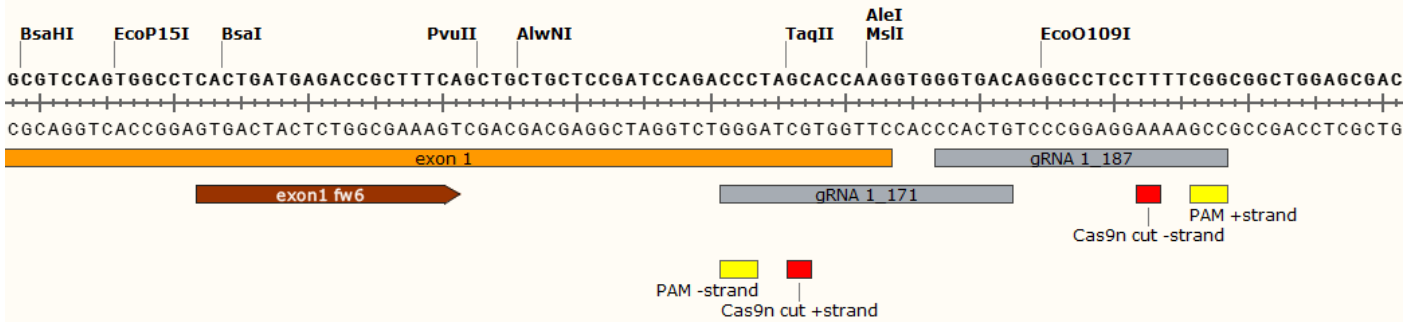
Clone #1 corresponds to #1 GLO^{-/-} in the manuscript



Clone #3 corresponds to #2 GLO^{-/-} in the manuscript



Clone #4 corresponds to #3 GLO^{-/-} in the manuscript



	GC GTCCAGTGGCCTCACTGATGAGACC... (exon 1) ... (gRNA 1 171) ... (gRNA 1 187)
Colony 1 (delta5)	cctcactgatgagaccgctttcagctgctgctccgatccagacc-----ccaaggtgggtgacagggcctccttttcggcggctggagcgac
Colony 2 (delta7)	cctcactgatgagaccgctttcagctgctgctccgatccagacc-----aaggtgggtgacagggcctccttttcggcggctggagcgac
Colony 3 (delta5)	cctcactgatgagaccgctttcagctgctgctccgatccagacc-----ccaaggtgggtgacagggcctccttttcggcggctggagcgac
Colony 4 (delta5)	cctcactgatgagaccgctttcagctgctgctccgatccagacc-----ccaaggtgggtgacagggcctccttttcggcggctggagcgac

Materials & Methods for Sequencing:

CRISPR genotyping via subcloning & sequencing of PCR product DNA was extracted from one well of 6-well plate for each clone with the Qiagen DNeasy blood & tissue kit (catalog #69506) according to manufacturer's recommendations for cells. A PCR product with primers covering 421 bp around the Cas9 cleavage site of sgRNA_171 (forward: 5'-GCTGGCCTGTTTGCTACTAG-3'; reverse: 5'-AGACACGGAATCTGACCCTG-3') was generated with the following PCR conditions: The PCR product was run on a 2% agarose gel, the band was cut and extracted with the Qiagen QIAquick gel extraction kit (catalog #28706) according to manufacturer's recommendations. 20 ng DNA of the eluate from the gel extraction was subcloned into the pJET1.2/blunt vector with the Thermo Fisher Scientific CloneJET PCR Cloning Kit (catalog #K1231) according to the blunting protocol of the manufacturer. 2.5 μ L of the ligation reaction per clone was transformed into chemocompetent *E. coli* (DH5 α) and plated on ampicillin-containing agar plates. At least four colonies per clone were picked, grown overnight in ampicillin-containing LB medium and DNA was extracted with the Qiagen QIAprep spin miniprep kit (catalog #27106) according to manufacturer's recommendations. 15 μ L of the recovered DNA at a concentration of 75 ng/ μ L and 2 μ L of a nested sequencing primer (pJET1.2 forward sequencing primer: 5'-CGACTCACTATAGGGAGAGCGGC-3') at a concentration of 10 μ M were mixed and sent for Sanger sequencing to Eurofins MWG Operon. The sequences obtained from Eurofins were analyzed with SnapGene software.

Loss of glyoxalase 1 induces compensatory mechanism to achieve dicarbonyl detoxification in mammalian Schwann cells

Jakob Morgenstern, Thomas Fleming, Dagmar Schumacher, Volker Eckstein, Marc Freichel, Stephan Herzig and Peter Nawroth

J. Biol. Chem. published online December 12, 2016

Access the most updated version of this article at doi: [10.1074/jbc.M116.760132](https://doi.org/10.1074/jbc.M116.760132)

Alerts:

- [When this article is cited](#)
- [When a correction for this article is posted](#)

[Click here](#) to choose from all of JBC's e-mail alerts

Supplemental material:

<http://www.jbc.org/content/suppl/2016/12/12/M116.760132.DC1.html>

This article cites 0 references, 0 of which can be accessed free at <http://www.jbc.org/content/early/2016/12/12/jbc.M116.760132.full.html#ref-list-1>